AFFDL-TR-79-3102

LEVEL (2)

AD A079008

ANALYSIS OF TRUNK FLUTTER IN
AN AIR CUSHION LANDING SYSTEM

FOSTER-MILLER ASSOCIATES, INC.
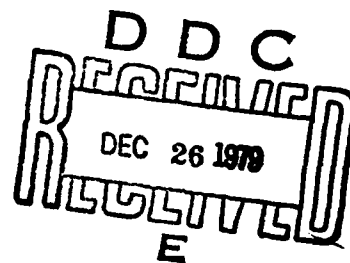*350 SECOND AVENUE*
WALTHAM, MA 02154

AUGUST 1979

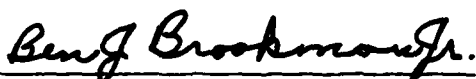TECHNICAL REPORT AFFDL-TR-79-3102
Final Report for period

AIR FORCE FLIGHT DYNAMICS LABORATORY
AIR FORCE WRIGHT AERONAUTICAL LABORATORIES
AIR FORCE SYSTEMS COMMAND
WRIGHT-PATTERSON AIR FORCE BASE, OHIO 45433

79 12 18 098

This technical report has been reviewed and is approved for publication.

Ben J. Brookman Jr.
Project Engineer

Howell K. Brewer
Chief, Mechanical Branch
Vehicle Equipment Division
AFFDL/FEM

FOR THE COMMANDER

A. B. Nutt
Director, Vehicle Equipment Divison
Air Force Flight Dynamics Laboratory

REPORT DOCUMENTATION PAGE		READ INSTRUCTIONS BEFORE COMPLETING FORM
1. REPORT NUMBER AFFDL-TR-79-3102	2. GOVT ACCESSION NO.	3. RECIPIENT'S CATALOG NUMBER
4. TITLE (and Subtitle) Analysis of Trunk Flutter in an Air Cushion Landing System.		5. TYPE OF REPORT & PERIOD COVERED Final rept.
		6. PERFORMING ORG. REPORT NUMBER WP-7819
7. AUTHOR(s) Ashok B. Boghani and Roger B. Fish		8. CONTRACT OR GRANT NUMBER(s) F33615-78-C-3412
9. PERFORMING ORGANIZATION NAME AND ADDRESS United States Air Force AFSC Aeronautical Systems Division Wright-Patterson AFB, Ohio 45433		10. PROGRAM ELEMENT, PROJECT, TASK AREA & WORK UNIT NUMBERS 2307N204 N2
11. CONTROLLING OFFICE NAME AND ADDRESS		12. REPORT DATE August 1979
		13. NUMBER OF PAGES 113
14. MONITORING AGENCY NAME & ADDRESS(if different from Controlling Office) 113		15. SECURITY CLASS. (of this report) Unclassified
		15a. DECLASSIFICATION/DOWNGRADING SCHEDULE

16. DISTRIBUTION STATEMENT (of this Report)

This document has been approved for public release and sale; its distribution is unlimited.

17. DISTRIBUTION STATEMENT (of the abstract entered in Block 20, if different from Report)

18. SUPPLEMENTARY NOTES

19. KEY WORDS (Continue on reverse side if necessary and identify by block number)

Air Cushion Landing System
Flutter
Air Cushion Vehicles

20. ABSTRACT (Continue on reverse side if necessary and identify by block number)

This report deals with explaining the occurrence of flutter in the Air Cushion Landing System (ACLS) trunks and suggesting means of suppressing it.

Observations of flutter in several ACLS trunks indicate that the flutter is caused by the interaction between the trunk membrane and the flow at the trunk bottom. The flow creates a negative stiffness effect

DD FORM 1473 EDITION OF 1 NOV 65 IS OBSOLETE
1 JAN 73

79 12 18 098

at the bottom which, if larger than the positive stiffness due to the tension of the trunk, induces flutter. A computer simulation based on this model succeeds in predicting the flutter observed in the XC-8A tests.

Suggestions on solving the flutter problem are based on either modifying the trunk or modifying the flow. Computer simulations of several suggestions indicate that:

(1) Providing a minimum gap

(2) Lowering the separation point

(3) Changing the operating conditions show good promise in suppressing the flutter.

Two other suggestions, not simulated, which also have good potential for flutter suppression are:

(1) Incorporating circular trunk

(2) Incorporating hybrid trunk.

FOREWORD

The work reported in this document was performed under Contract No. F33615-78-C-3412, Trunk Flutter Analysis. The technical project officer of the project was Mr. B.J. Brookman, Jr. The authors wish to acknowledge the assistance of Dr. A. Erickson and Dr. D. Wormley in performance of the contract.

TABLE OF CONTENTS

TABLE OF CONTENTS (Continued)

LIST OF ILLUSTRATIONS

LIST OF ILLUSTRATIONS (Continued)

LIST OF TABLES

Principal Nomenclature

A	Gap area per unit width under the trunk
A_o	Trunk orifice area
A_{ta}	Trunk-to-atmosphere orifice area
A_{tc}	Trunk-to-cushion orifice area
A_{tr}	Trim valve area
B_ℓ	Trunk flexural damping constant
C_d	Trunk orifice discharge coefficient (generally same as C_{ta} and C_{tc})
C_{ta}	Trunk-to-atmosphere discharge coefficient
C_{tc}	Trunk-to-cushion discharge coefficient
C_{tr}	Trim valve discharge coefficient
h	Gap height
h_1	Minimum gap height
h_2	Gap height at flow separation
I_{fan}	Inertance of air in the fan and the duct
k	Polytropic constant
K_ℓ	Trunk flexural stiffness constant
P	Pressure under the trunk

P_a	Atmospheric pressure
P_c	Cushion pressure (gauge)
P_{fan}	Fan discharge pressure (gauge)
P_t	Trunk pressure (gauge)
P_1	Pressure under the trunk at the minimum gap height
R	Trunk radius of curvature
Q	Volume rate of cushion flow per unit width
Q_{ca}	Total cushion flow
Q_{fan}	Fan flow
Q_{ta}	Total trunk-to-atmosphere flow
Q_{tc}	Total trunk-to-cushion flow (not including the trim valve flow)
Q_{tr}	Total trim valve flow
v	Flow velocity under the trunk
V_c	Cushion volume
V_t	Trunk volume
v_o	Flow velocity at beginning of trunk bottom zone (approximately $= 0$)

v_1	Flow velocity at the minimum gap height
v_2	Flow velocity at the separation point
w	Mass rate of flow per unit width
w_ℓ	Mass rate of trunk orifice flow
$\alpha_o - \alpha_4$	Fan characteristic polynomial
θ	Trunk slope at separation point
ψ	Angle between the two trunk links in the lumped mass model
ϕ	Trunk Slope
τ_B	Flexural damping torque
τ_K	Flexural stiffness torque.

1. INTRODUCTION

1.1 General

This is the final report on Contract No. F33615-78-C-3412, Trunk Flutter Analysis. The objective of the contract was to gain understanding of the basic mechanism of flutter observed in the Air Cushion Landing System (ACLS) trunk and to develop a computer simulation to assist in designing flutter free trunks.

This report is accompanied by a film showing flutter in a typical ACLS. The computer programs developed as a part of the contract are described in another document (1).

1.2 Background

Flutter resulting from fluid flow - structural interactions - has been studied for many years. Extensive study of lifting surface and control surface flutter resulting from aerodynamic forces coupling with structural elastic properties has resulted in development of analytical techniques that have been very successful in guiding the design of flutter-free aircraft structures.

Local vibration of shell and plate type structures, usually referred to as "panel flutter," typically has structural characteristics determined by stiffness due to bending. In some cases tension has been considered as a secondary effect. Theoretical calculations of panel flutter have had moderate success when compared with experimental results, particularly if care is taken to match the theoretical and experimental boundary conditions. Overall correlations of experimental and theoretical results for panel flutter are not as good as comparisons for lifting surface flutter.

1

Air cushion trunk flutter differs considerably from lifting surface flutter and panel flutter. It is characterized by the interaction between the fluid flow field and an elastic membrane in which the primary structural parameter is the membrane tension. This type of flutter problem has similarities to the membrane flutter problems studied by Kelvin, Rayleigh and Lamb (2) as exhibited in waving of flags, sail vibration and waves between two layers of liquid with surface tension at the interface. Trunk flutter also differs from panel flutter in that the fluid flow field in the former is very strongly affected by flow separation downstream of the minimum gap area.

Trunk membrane flutter has been a problem with almost all scale model and full-scale prototype air cushion trunks fabricated over the last 10 years. For example, the prototype scale model ACLS fabricated by Boeing (3), Jindink ACLS (4) and XC-8A (5) have all suffered from trunk flutter.

Many efforts have been made in the past to study flutter. From an experimental study, Bass and Johnson (6) came to a conclusion that skirt flutter is initiated when the velocity in the trunk to ground gap reaches a sufficient magnitude. The threshold velocity was shown to vary with trunk pressure, trunk geometry, trunk flow and the surface characteristics. Han (7) investigated the available flutter data from a number of ACLS tests and found that there was no particular correlation between the natural frequencies of trunk membrane and the flutter frequencies. He also suggested that the flutter was caused by vortex shedding which led to pressure fluctuations on the trunk side giving rise to flutter. In an investigation directed chiefly towards eliminating flutter in the Jindivik ACLS, Forzono (8) concluded that for a flutter free ACLS the cushion mass flow should be kept to a minimum and trunk flow should be kept to a maximum. He further demonstrated that if several channels were provided under the trunk to allow the cushion air to escape, flutter could

be eliminated. Fowler (9), after studying flutter in a light air cushion vehicle, concluded that the flutter could be suppressed by a device known as Buzz-Dinger array which essentially involved attaching lead shots to the skirt.

Thus, most of the past projects have been experimentally oriented and no serious attempts have been made to understand the basic flutter mechanism. Bell has performed some initial analytical work on flutter (10). However, the details of the work are not available.

What is needed then is a study which attempts to understand the basic flutter mechanism. Once the cause of the flutter is analytically explained, designing a flutter free trunk would be a more rational task not dependent on the trial-and-error methods used until now. The work described in this report initiates such an effort.

1.3 Summary

As the first task of the project, two different ACLS's were studied in order to determine the cause of flutter (see Section 2).

a. ACLS for XC-8A
b. A prototype ACLS belonging to NASA currently at FMA.

Trunk flutter in XC-8A was studied from the films, interface technical memorandum, the test data and the available literature. The flutter in the prototype ACLS, on the other hand, was filmed with a high speed camera and several measurements with pressure gauges and accelerometers were taken.

Some of the inferences arrived at from such a study were:

a. The motion of the trunk bottom seems to be the most
    important element in the flutter.

b. The flutter motion originates at the bottom and propa-
    gates to the sides.

c. The forcing function causing flutter sometimes excites
    more than one mode of trunk vibration.

d. The flutter is suppressed if the air cushion is vented
    out either by mounting strips under the trunk or
    through operation over rough surface such as grass.

e. The flutter frequencies and modes of vibration are
    dependent on the load.

Based on these observations it seems that the flutter
is caused by effects of fluid flow at the bottom of the trunk
and not by vortex shedding on the trunk sides. The
basic flutter model then developed describes the flow under the
bottom by Bernoulli's equation in order to obtain the pressure
acting at the trunk bottom as discussed in Section 3. (This
pressure profile was verified through a test performed at FMA as
described in Appendix A.) By evaluating the effects on the pres-
sure profile due to a small perturbation, a negative stiffness
effect on the trunk bottom caused by the flow is determined.
If this negative stiffness is larger than the positive stiffness
due to trunk tension, flutter is initiated. This can explain
the effects of various parameters on flutter identified in the
XC-8A tests. The accuracy of the basic model is then improved
by including the effects of trunk-cushion-fan flow dynamics,
trunk flexural stiffness and trunk orifice flow.

A computer program developed based on the model is able to predict the occurrence of flutter in the XC-8A. The frequency of flutter is also predicted reasonably well as described in Section 4.

The suggestions on suppressing flutter, discussed in Section 5, are based on reducing the negative stiffness or increasing the positive stiffness either through changes in the flow or through changes in the trunk characteristics. Generic types of flutter suppression methods discussed in Section 5 are:

- Modifying Trunk

    - Increasing stiffness at trunk bottom
    - Increasing flexural stiffness
    - Increasing hoop stiffness
    - Incorporating hybrid trunk

- Modifying Flow

    - Lowering separation point
    - Providing a gap under the trunk
    - Changing the operating conditions.

Computer simulations run for all but two of these methods evaluate their flutter-suppressing effects.

The report ends with the conclusions and recommendations. Two of the recommendations are:

- Further study of the separation point location during flutter is required

- The flutter suppressing methods need to be studied further.

2. FLUTTER OBSERVATIONS

In order to identify the characteristics of flutter, the performance of two different ACLS was studied:

a. XC-8A

b. Prototype ACLS at FMA.

There are two major differences between the two ACLS; the size and the elasticity of the trunk. The XC-8A trunk, which was designed to hug the fuselage of the aircraft when not pressurized, exhibited a nonlinear elastic characteristic, whereas the trunk of the prototype ACLS at FMA is essentially inelastic. In spite of this difference, both trunks have exhibited high frequency "flutter" motion in certain situations as described in the following pages.

2.1 XC-8A Data

The XC-8A test program data supplied by WPAFB were analyzed. These data were selected based on their potential usefulness to understanding the occurrence of flutter in XC-8A. The tests for which the data were obtained (in form of test summaries and films) are summarized in Table 1. In addition, the related interface technical memorandum, XC-8A ACLS test calendar, test list from draft of AFFDL-TR-78-61 were obtained.

These data were studied in view of identifying the nature of the problem. Conclusions reached from this study are:

a. A number of high-frequency phenomena which could be classified as flutter (in the air cushion trunk context and not strictly as defined in aerodynamics) were observed in the films.

6

TABLE 1.   THE FLUTTER RELATED TESTS BEING STUDIED

Test	Description
Trunk No. 2	
S - 092574-1	Trunk oscillation with CG shift
S - 100274-1	Trunk oscillation with mass damper
S - 110774-1	Trunk oscillation with re-designed strakes
S - 021275-1	Trunk oscillation
T - 030475-1	Low speed taxi
FT - 061975-1	Grass landing - take off
Trunk No. 3	
S - 090876-2	Trunk oscillations for trunk No. 3
S - 012677-1	Antiflutter modification check
S - 020877-1	Modification antiflutter modification check
S - 021777-2	CG shift effect on flutter
S - 031177-1 and 2	Ground feelers check
S - 031477-1	Tow test on grass and hard surface

b.   The most prominent mode of flutter in the XC-8A trunk
     was shown in the figure below

                                            SLAPPING ON
                                            THE GROUND
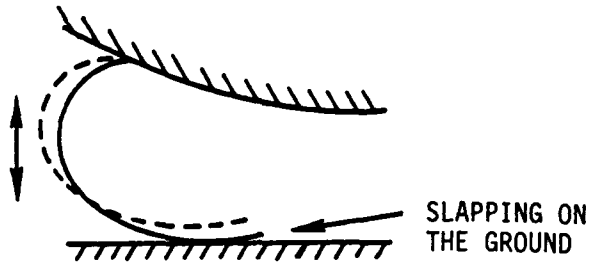
c.   The most common place for the flutter to occur was at
     the transition between the curved and the straight
     sections on the front part of the trunk

d.   Sometimes the flutter seemed to follow a two-frequency
     behavior such as:

     This behavior was also observed in Jindivik and 2-D
     section tests by Forzono

e.   Occasionally, the complete side trunk exhibited flutter-
     like movement

f.   Sometimes a flutter propagation along the trunk length
     was observed
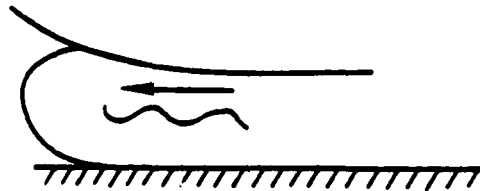
g. Heave oscillations of the aircraft sometimes occurred
    with the flutter, sometimes without

h. Most of the flutter suppression devices, such as mass
    dampers, strakes, fingers, tape restraining system,
    etc. were unsuccessful or only partly successful. The
    strips under the trunk, however, prevented the trunk
    from fluttering.

The effects of various parameters on flutter were compiled
from the above observations and from the literature. These
effects are summarized in Table 2.

2.2 FMA Tests

The ACLS at the Saxonville facility of FMA shown in Figure 1
also exhibits flutter. This flutter was studied further using
pressure gauges, accelerometers and displacement transducers.
In addition a high speed (1000 frames/sec) film was made
to study and document flutter. Figure 2 shows details of the
ACLS. The trunk of this ACLS is made from dacron coated with
polyurethane and it is 15 mm thick.

Two sets of tests were performed on this ACLS. In the first
test, the load on the ACLS was increased from 100 to 346 lb and
the pressure under the trunk was monitored through five pressure
taps mounted as shown in Figure 3. A typical chart record for a
test with total load of 190 lb is shown in Figure 4. As shown
in the figure, the flutter is accompanied by violent changes in
the pressure under the trunk.

In addition, we observe:

a. The pressure fluctuation under the trunk is the
    largest at the center and tapers off at both ends.

TABLE 2. EFFECTS OF VARIOUS PARAMETERS ON FLUTTER

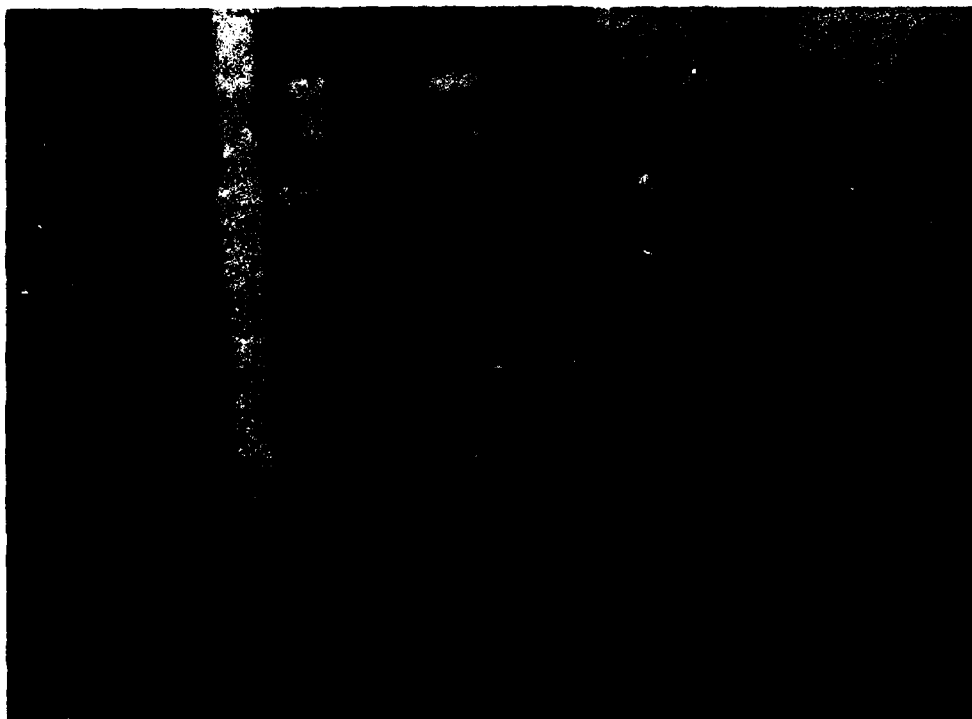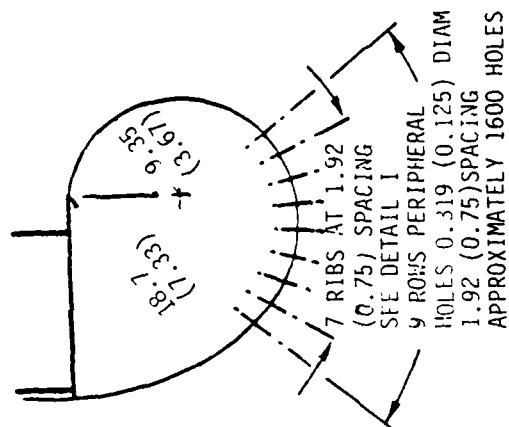| No.	Parameter	When it is	Flutter ....
1.	Trunk pressure	Increased beyond 270 to 350 psfg	Increases
2.	Trim ports	Changed 15 open	Threshold* changes threshold P_t = 325 psfg
		5 open	threshold P_t = 315 psfg
3.	Pillow brakes	Applied	Generally reduces
4.	Wind	Increased	Generally increased
		Head wind	Destabilizes
		Tail wind	Stabilizes
5.	Inertial Dampers	Attached	Threshold pressure does not change but the amplitude reduces.
6.	Strakes	Attached	Threshold pressure increases to 278 to 310 psfg.
7.	Terrain	On grass	Suppressed
		On smooth surface	Violent
8.	CG location	Moved forward when pitch-up attitude	Threshold pressure increases slightly
9.	Forward motion	Increased	Reduces (claimed by Bell)
10.	Turning maneuvers	Executed	Promoted on high wing forward portion of the trunk on outer radius of turn.

* Threshold is defined as the trunk pressure value beyond which the trunk flutters.
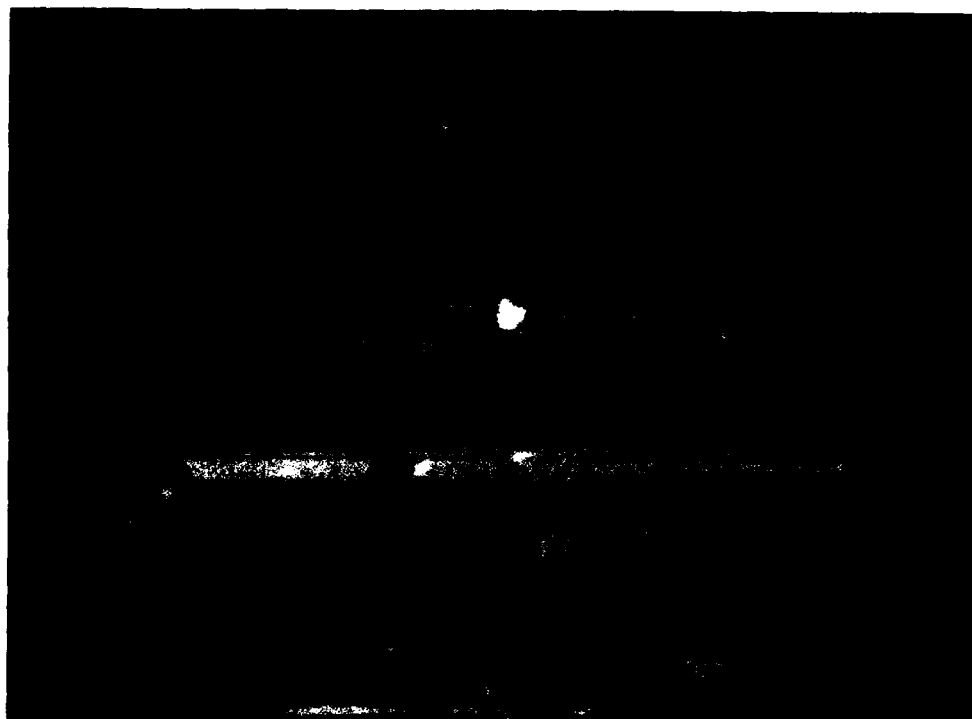
A. THE TEST STAND (FABRICATED FOR TESTS
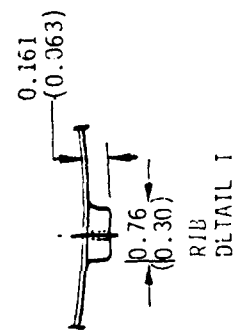UNDER NASA CONTRACT NAS1-12403)

B. HIGH SPEED FILMING OF THE ACLS FLUTTER

Figure 1. The ACLS at FMA.

11

SECTION A-A

7 RIBS AT 1.92
(0.75) SPACING
SEE DETAIL I

9 ROWS PERIPHERAL
HOLES 0.319 (0.125) DIAM
1.92 (0.75)SPACING
APPROXIMATELY 1600 HOLES

16.9
(6.9)

18.1
(7.33)

DIMENSIONS IN cm(in.)

0.161
(0.363)

0.76
(0.30)

RIB
DETAIL I

C. TRUNK DETAILS

FAN

PLENUM

TRUNK

161
(63)

71 (28)

DIMENSION IN cm(in.)

A. SIDE VIEW

10.2
(4.0)

A

A

94
(37)
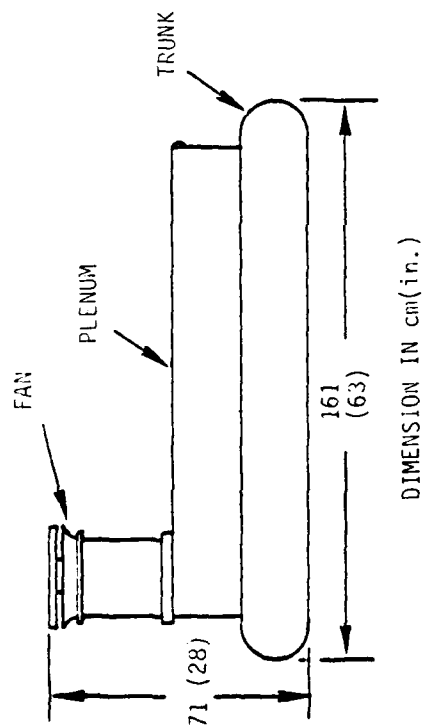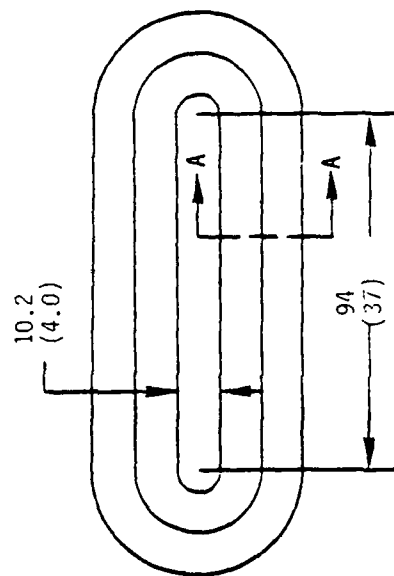
B. BOTTOM VIEW

Figure 2. The Test Cushion.

12
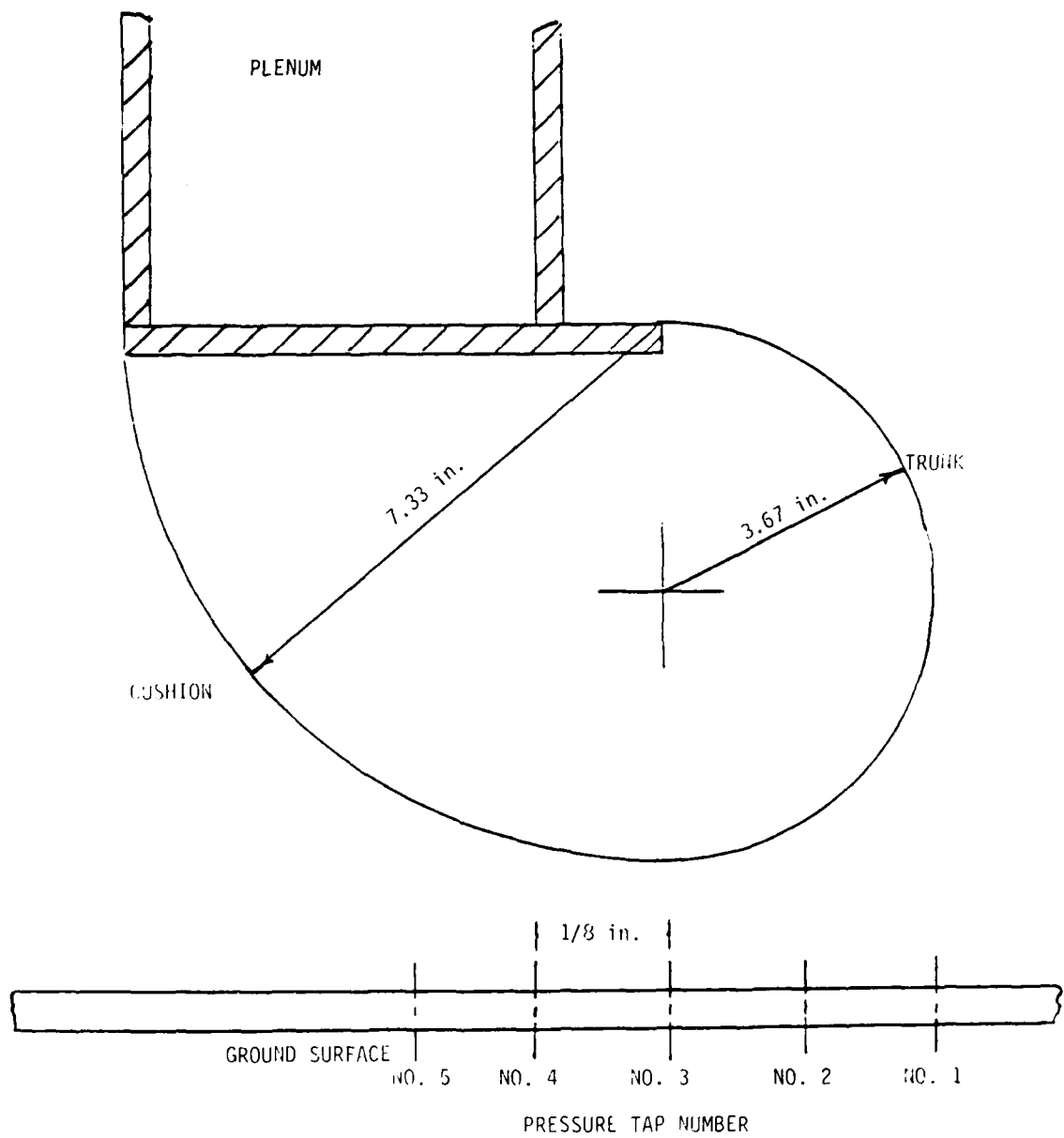
Figure 3. Location of the Pressure Taps Under the Trunk.

13
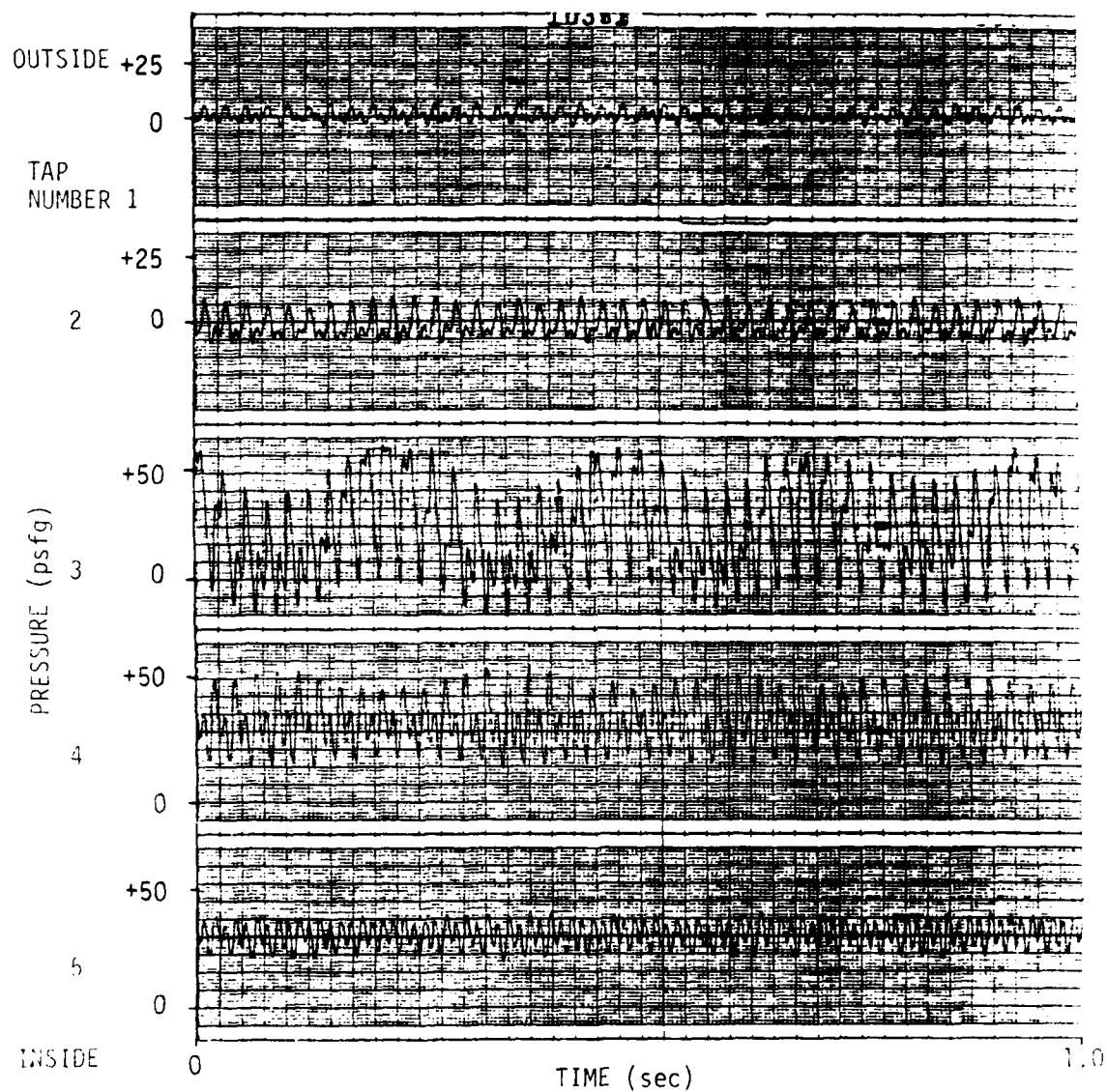
Figure 4. Flutter Performance of the FMA ACLS at 190 lb, Pressure Profile Under the Trunk.

14

The primary frequency of fluctuations is 42 Hz. In addition, a higher mode vibration at 84 Hz is superimposed.

b.   The pressure under the trunk also varies due to gross oscillations of the trunk lobe at the heave natural frequency ($\simeq$ 4 Hz).

Figure 5 shows variations in pressure under the trunk for tests performed at various loads. These results show:

a.   For the loads at which the tests were performed, the amplitude of the flutter increases as the load is increased to 190 lb, then reduces to almost zero at a 268 lb load. If the load is further increased, the flutter reappears at a higher frequency (130 Hz). This may mean a change in the mode of vibration beyond a certain limit on the load

b.   There is a slight increase in the flutter frequency (40 to 44 Hz) as the load is increased from 100 to 229 lb.

During the second set of tests, we mounted pressure transducers under both side trunks and in the cushion, plenum, and trunk. In addition, a small accelerometer was mounted on the right side trunk. The load was then changed from 190 to 346 lb and the resulting variations in the parameters were recorded as shown in Figures 6 through 9. From these plots we observe:

a.   The pressures under the two side trunks vary quite differently. This may be due to a slight roll attitude of the ACLS resulting into a difference in the nominal gap height under the two sides. In fact, at any load the left side trunk has a larger gap height than the right side trunk. Therefore, when
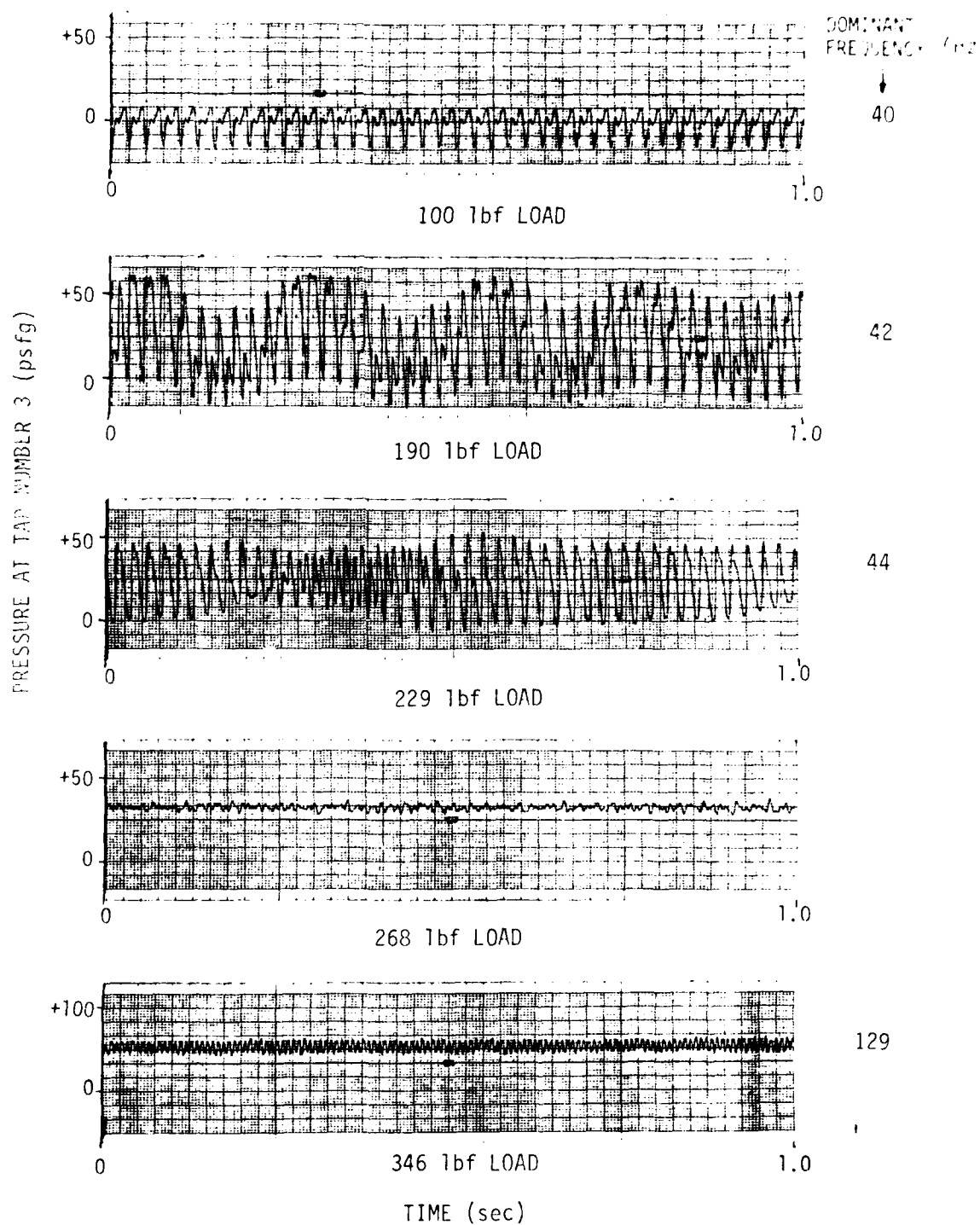
15

Figure 5.   Effect of ACLS Load on Pressure Variation
Under the Trunk During Flutter.

16

Figure 6. Flutter on FMA ACLS at 190-lb load.

17

PLENUM
PRESSURE
(psfg)

100 —

0 —

TRUNK
PRESSURE
(psfg)

100 —

0 —

CUSHION
PRESSURE
(psfg)

50 —

0 —

LEFT SIDE
UNDERTRUNK
PRESSURE
(psfg)

35 —

0 —

RIGHT SIDE
UNDERTRUNK
PRESSURE
(psfg)

35 —

0 —

RIGHT TRUNK
LATERAL
ACCELERATION
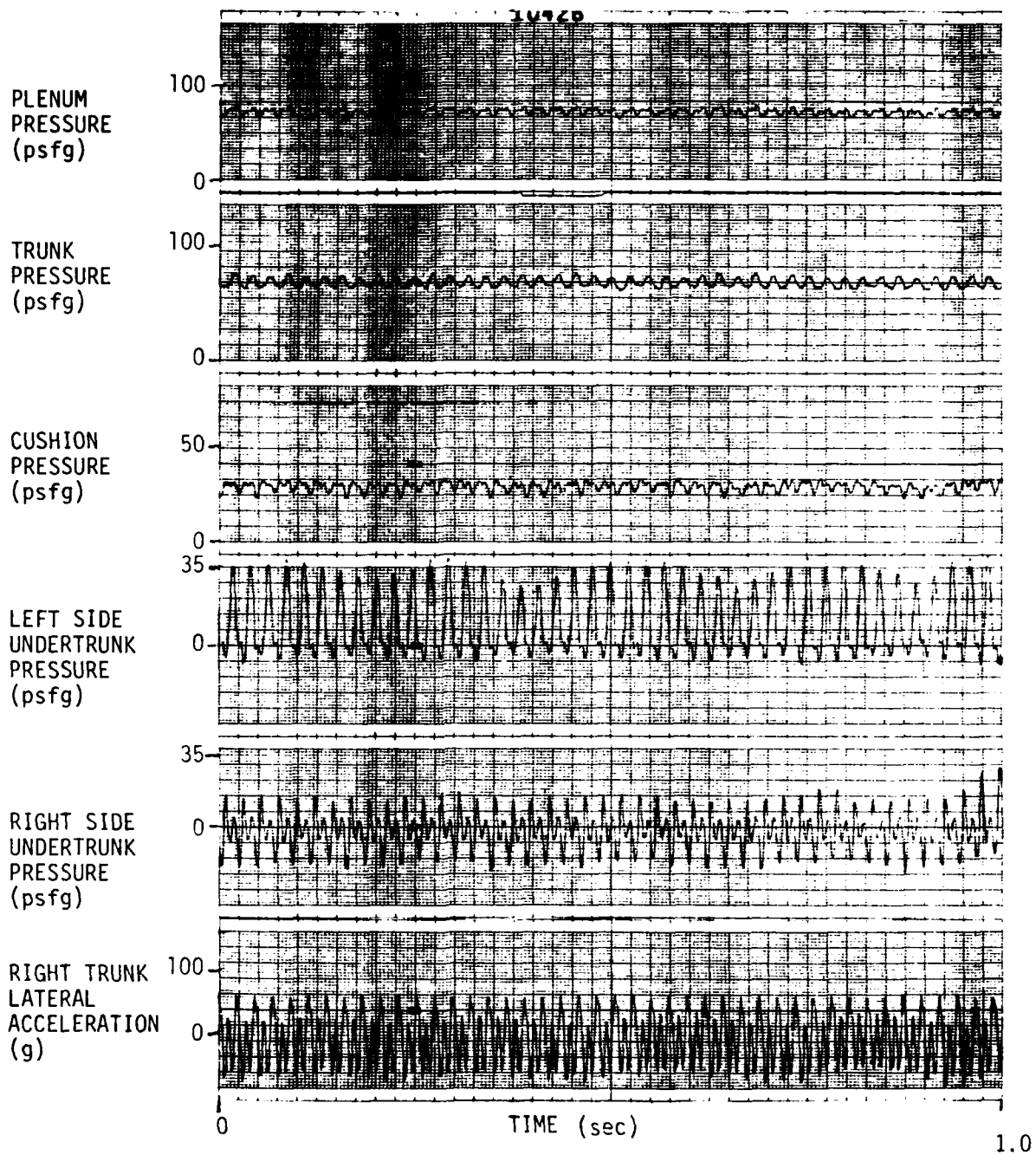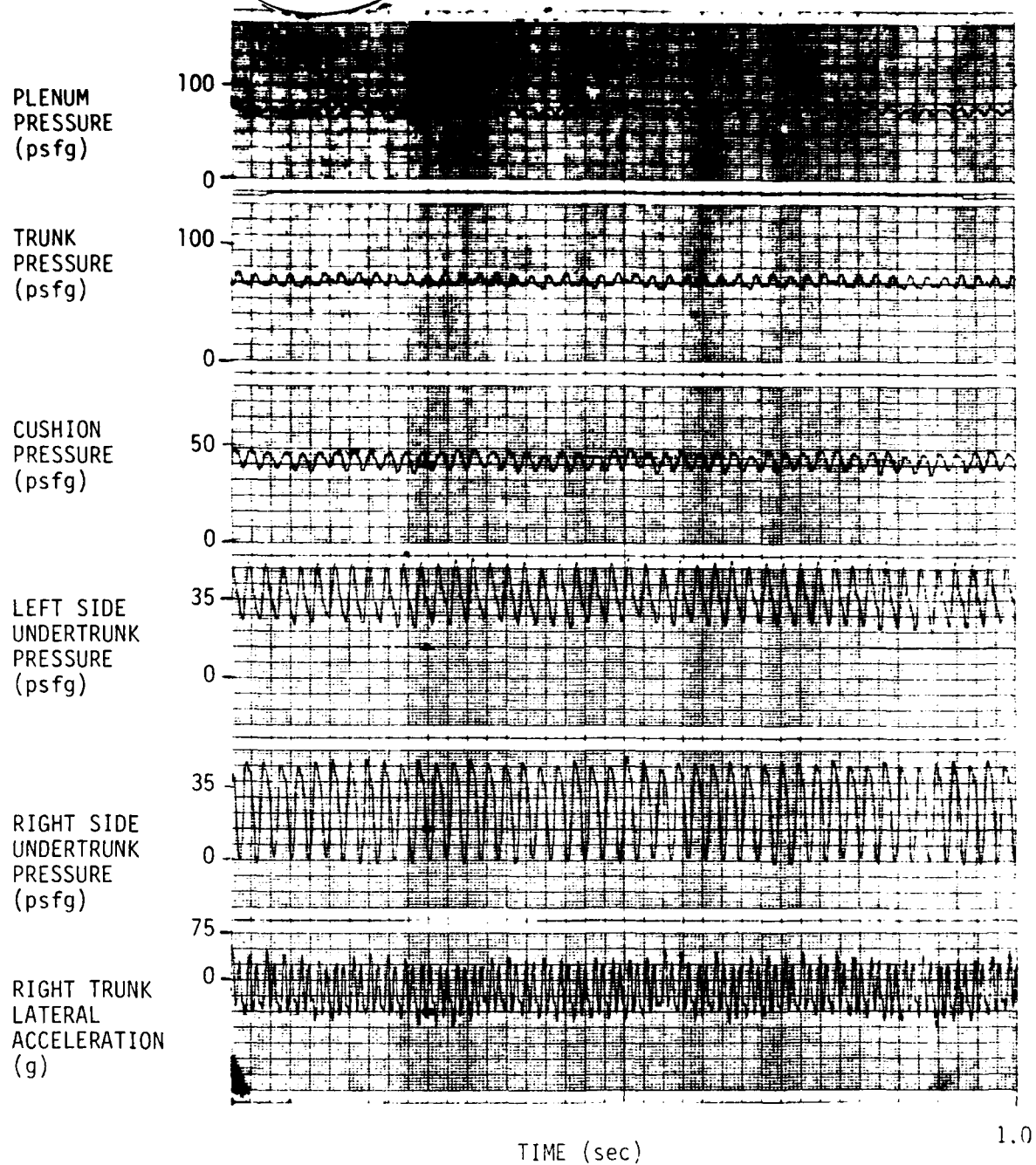(g)

75 —

0 —

TIME (sec)

1.0

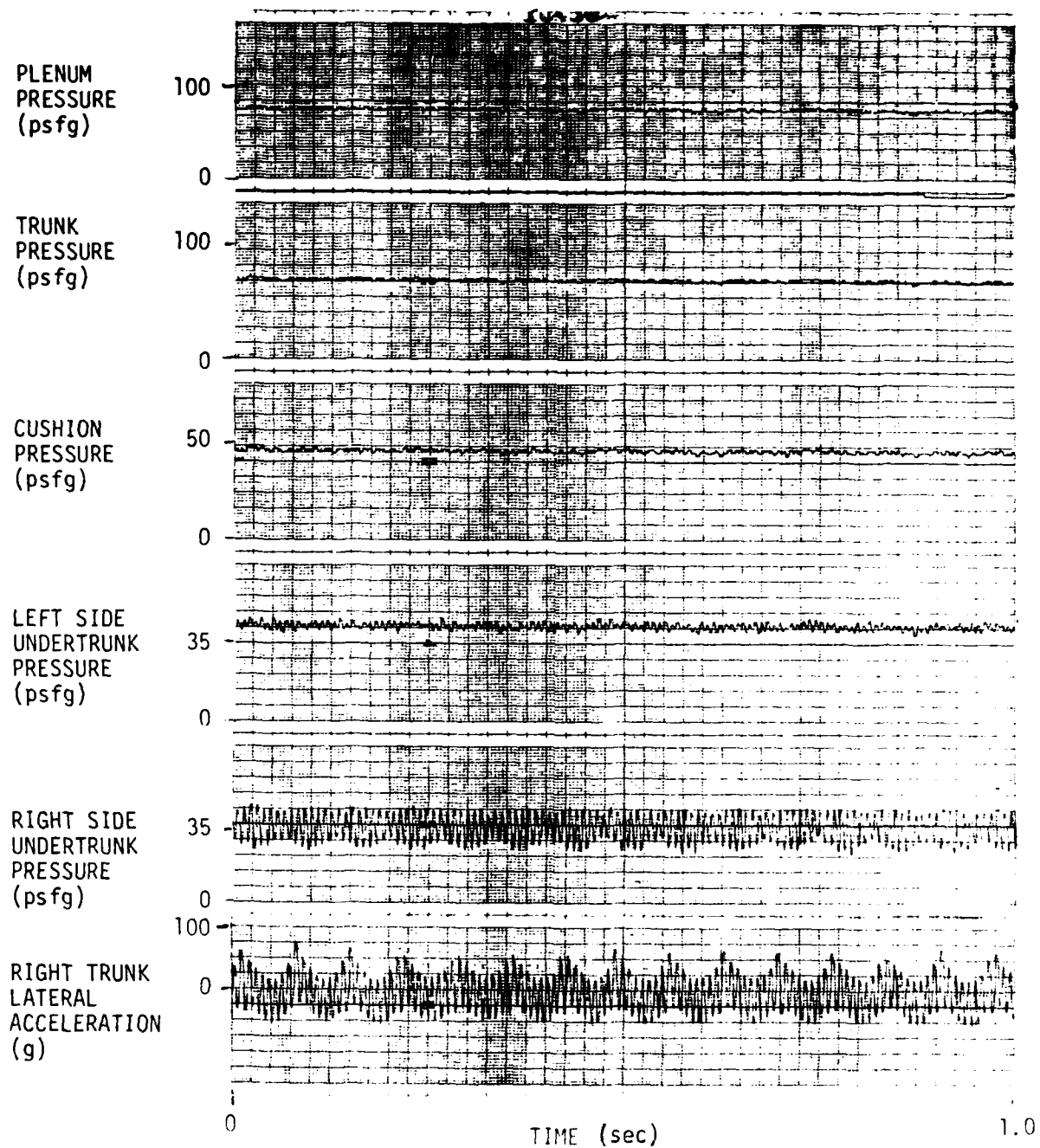Figure 7.   Flutter on FMA ACLS at 268-lb load.

18

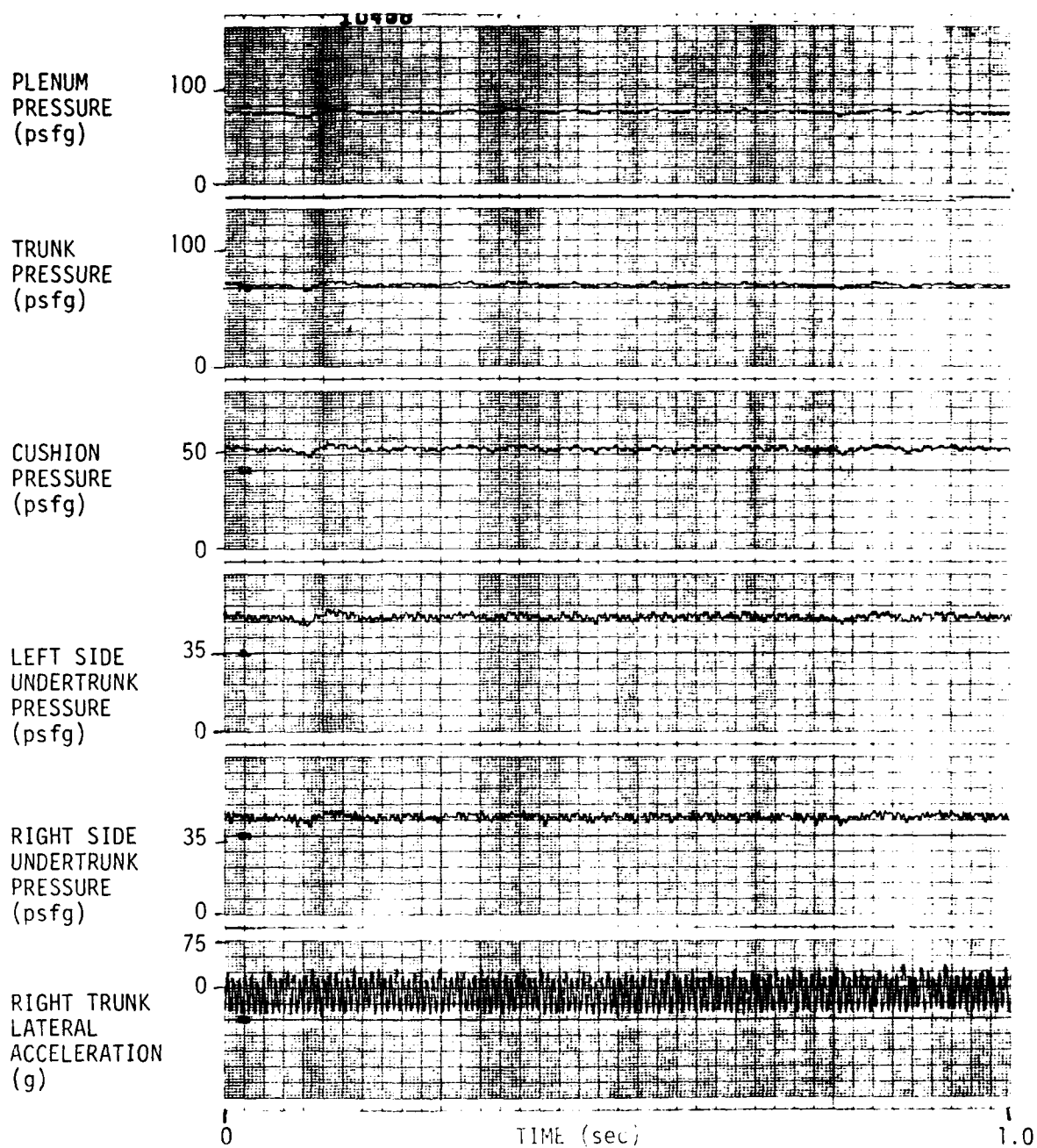Figure 8. Flutter on FMA ACLS at 310-lb load.

Figure 9. Flutter on FMA ACLS at 346-lb load.

20

the load is increased to 268-lb, the right trunk has
the same gap height as what the left side trunk had for
a 190-lb load. This gives rise to a similarity in the
pressure profile for the left side trunk for a 190-lb
load and the right side trunk for a 268-lb load.

b.   The shape of vibration of the left side trunk at 190-lb
      load was as shown below:
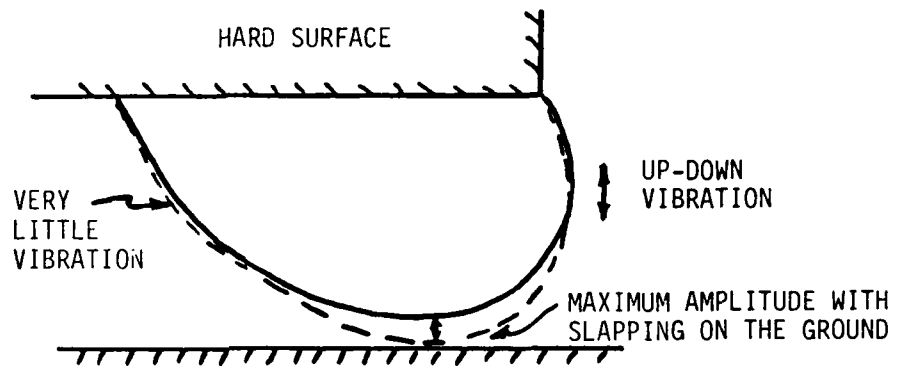
As shown, the largest amplitutde of vibration occurs at
the bottom of the trunk. The inner side of the trunk
vibrates very little and only in a longitudinal direc-
tion, whereas the outer side moves up and down instead
of moving laterally. Therefore the overall motion is
two-dimensional (not pure lateral or longitudinal) and
it seems to be caused by severe pressure at the bottom
of the trunk. This primary mode of vibration changes
when the load is increased.

    In order to study the flutter motion further, a high speed
(1000 frames/sec) film was made. This film, supplied with
the report, included shots of the trunk flutter from various an-
gles and for different loads.

21

The film confirms the observations made earlier; namely, the flutter tendency depends on the load. There is an instability when the load is increased, beyond which the flutter tendency is sharply less. The film also shows a plate-like motion of the trunk bottom where the bottom assumes a flat profile and slams on the ground, exciting various modes of vibrations in the trunk.

From these observations a flutter model was developed as discussed in the next section.

3. FLUTTER MODEL

The observations of flutter described in Section 2 lead us to believe that the bottom of the trunk is involved significantly in the occurrence of flutter. The flutter is caused by variations in the pressure profile under the trunk giving rise to motion of the trunk bottom, which then causes the trunk sides to move at the same time. Because of the severity of the trunk motion and involvement of the trunk bottom, we do not believe that vortex shedding on the side of the trunk (7) causes flutter.

This section outlines a flutter model that was developed based on this assumption. As shown later, a model thus developed is able to explain the flutter characteristics quite well. Initially, a basic flutter model which deals with behavior of a pressurized membrane with a flow underneath is developed. In the latter part of the section various other effects such as the cushion-trunk-fan air dynamics, flexural stiffness of the trunk and the trunk orifice flow are incorporated in the basic model.

3.1 Description of the Basic Model

The basic model assumes:

a. The cushion cavity is a constant pressure source where the streamlines to the atmosphere originate.

b. The flow from the trunk orifices does not significantly affect the flow-pressure relationship of the cushion atmosphere flow.

c. The fluid is incompressible.

d. The curvature of the trunk does not affect the flow.

Then the steady-state Bernoulli's equation for the region under points B and C in Figure 10 gives:

$$P_C = P + 1/2 \, \rho v^2 = P_1 + 1/2 \, \rho v_1^2$$

$$= P_a + 1/2 \, \rho v_2^2 \qquad (1)$$

and from the flow continuity equation

$$Q = v_1 h_1 = v_2 h_2 = vh \qquad (2)$$

where Q is flow per unit length of the trunk.

If h_1/h_2 is assumed to be K_1, then from equation (2),

$$v_2 = v_1 \frac{h_1}{h_2} = v_1 K_1 \qquad (3)$$

From equation (1),

$$P_C - P_a = 1/2 \, \rho v_2^2 = 1/2 \, \rho K_1^2 v_1^2 \qquad (4)$$

and

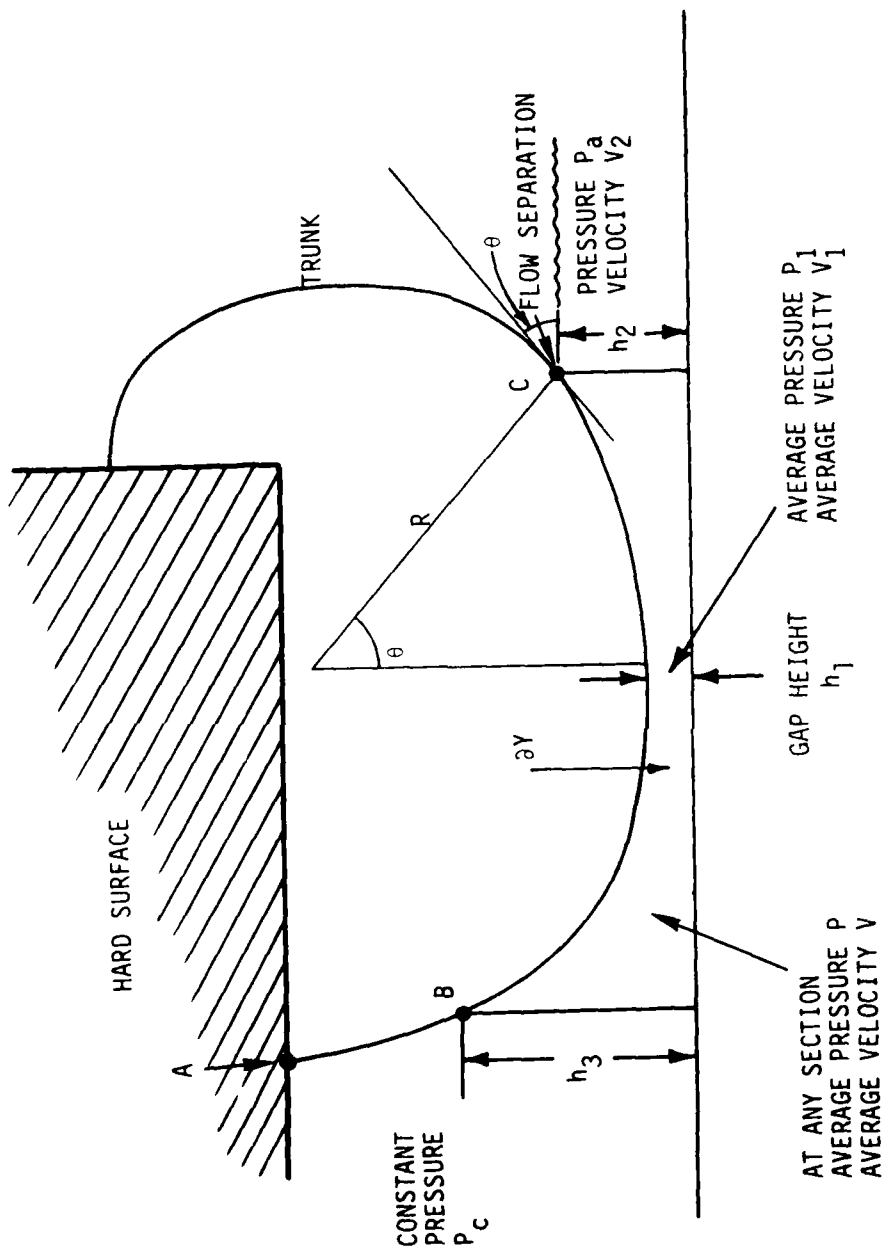$$P_1 = P_C - 1/2 \, \rho v_1^2 = P_C - \frac{P_C - P_a}{K_1^2} \qquad (5)$$

24

Figure 10. The Fluid Model Being Incorporated in the Simulation Program.

Similarly,

$$P = P_c - \frac{P_c - P_a}{K^2} \qquad (6)$$

where

$$K = \frac{h}{h_2}$$

This equation is verified experimentally as shown in Appendix A. Such verification also proves that the curvature of the trunk need not be taken into account while determining the pressure profile under the trunk.

For displacement ∂Y, shown in Figure 10,

$$\frac{\partial P_1}{\partial Y} = \frac{\partial P_1}{\partial K_1} \cdot \frac{\partial K_1}{\partial Y} \qquad (7)$$

Evaluating $\partial K_1 / \partial Y$ in this expression requires knowledge of where the separation point will move when the trunk shape is changed for perturbation ∂Y. We are not certain of what would happen and further tests are required before the behavior of the separation point is completely understood. For the purpose of this study we have made two different assumptions and have evaluated equation (7) for both. These assumptions are:

a. Separation point height, h_2, remains constant for any motion of the trunk in this case:

26

$$\frac{\partial P_1}{\partial Y} = \frac{2(P_c - P_a)}{K_1^3} \left(- \frac{1}{h_2}\right) \tag{8}$$

$$\frac{\partial P_1}{\partial Y} = - \frac{2(P_c - P_a) h_2^2}{h_1^3} \tag{9}$$

b. Alternately, the angle θ at which the separation takes place can be assumed to remain constant. In this case

$$h_2 = h_1 + R(1 - \cos \theta) \tag{10}$$

assuming that the trunk cross section on the atmospheric side is circular with radius R.

If $K_2 = h_2/h_1$

Then

$$K_2 = 1 + \frac{R}{h_1} (1 - \cos \theta) \tag{11}$$

27

From equation (5)

$$P_1 = P_c - K_2^2 (P_c - P_a) \qquad (12)$$

Also

$$\frac{\partial P_1}{\partial Y} = \frac{\partial P_1}{\partial K_2} \cdot \frac{\partial K_2}{\partial Y} \qquad (13)$$

However

$$\frac{\partial P_1}{\partial K_2} = - 2K_2 (P_c - P_a) \qquad (14)$$

$$\frac{\partial K_2}{\partial Y} = 0 + \frac{\partial}{\partial Y} \frac{R}{h_1} (1 - \cos \theta) \qquad (15)$$

But since θ is constant

$$\frac{\partial K_2}{\partial Y} = (1 - \cos \theta) \frac{\partial}{\partial Y} \frac{R}{h_1} \qquad (16)$$

$$\frac{\partial K_2}{\partial Y} = (1 - \cos \theta) \left(\frac{h_1 \frac{\partial R}{\partial Y} + R}{h_1^2} \right) \tag{17}$$

(Since $\partial h_1 / \partial Y = -1$)

Substituting the values of $\partial P_1 / \partial K_2$ and $\partial K_2 / \partial Y$ from equations (14) and (17) respectively, in equation (13),
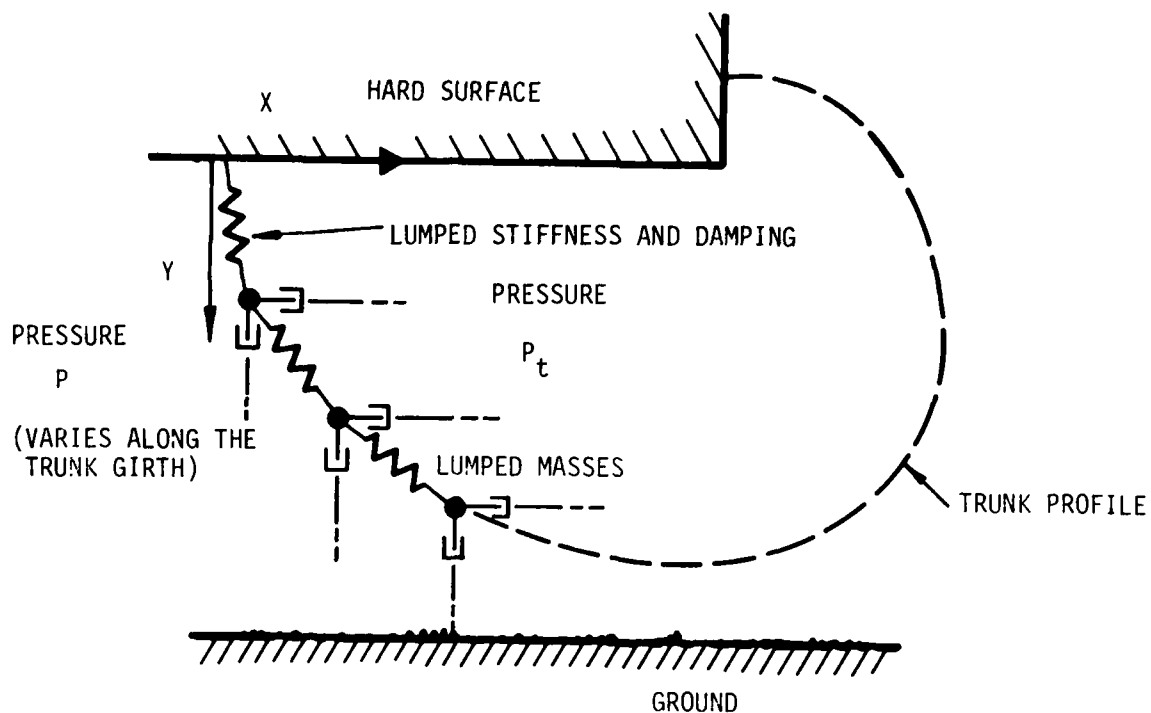
$$\frac{\partial P_1}{\partial Y} = -2 \frac{h_2}{h_1} (P_c - P_a) (1 - \cos \theta) \frac{\left(h_1 \frac{\partial R}{\partial Y} + R \right)}{h_1^2} \tag{18}$$

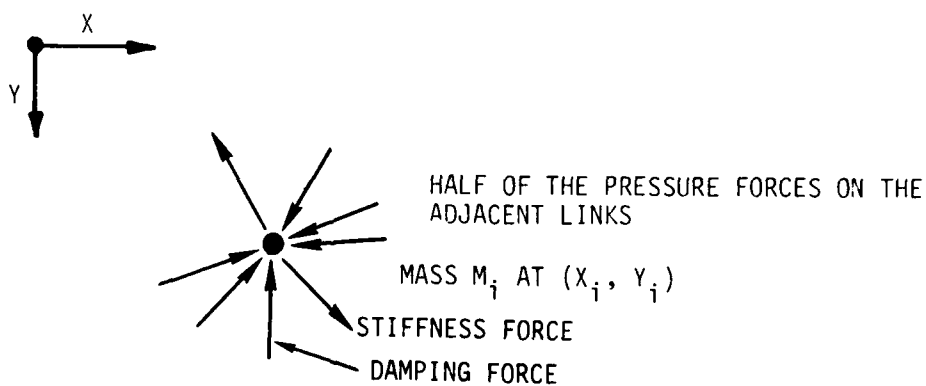However, $h_2 = h_1 + R(1 - \cos \theta) \simeq R(1 - \cos \theta)$

Therefore,

$$\frac{\partial P_1}{\partial Y} \simeq -2 \frac{R}{h_1^3} (P_c - P_a) (1 - \cos \theta)^2 \left(h_1 \frac{\partial R}{\partial Y} + R \right) \tag{19}$$

The trunk model represents the trunk as made of lumped masses connected with linear springs as shown in Figure 11. The masses also have global dampers to simulate damping effects.

HARD SURFACE

LUMPED STIFFNESS AND DAMPING

PRESSURE

P_t

PRESSURE

P

(VARIES ALONG THE
TRUNK GIRTH)

LUMPED MASSES

TRUNK PROFILE

GROUND

A. LUMPED PARAMETER REPRESENTATION OF THE TRUNK

X

Y

HALF OF THE PRESSURE FORCES ON THE
ADJACENT LINKS

MASS M_i AT (X_i, Y_i)

STIFFNESS FORCE

DAMPING FORCE

B. FORCE BALANCE OF THE ITH LUMPED MASS

Figure 11. Basic model of the trunk.

30

The forces acting on the lumped masses include the damping forces, stiffness forces and the pressure forces (which are assumed to act perpendicular to the lines joining the lumped masses). The pressure forces acting on each link between the masses are divided between the adjacent masses.

The initial positions of the masses are determined from the initial trunk shape. The subsequent positions, expressed in X and Y coordinates, are determined from the differential equations relating the accelerations along the two coordinate axes and the force components.

3.2 Stability of the Basic Model

With either assumption regarding separation point, equations (9) and (19) indicate that a negative stiffness is created by the flow under the trunk. This is quite apparent if h_2 is assumed to be constant as in equation (9). For the assumption that the trunk slope at the separation point stays constant, whether a negative stiffness exists or not depends on $\partial R/\partial Y$, which represents the change in trunk curvature as the lowest point on the trunk is moved. This could be zero or negative, depending on behavior of the rest of the trunk. However if $h_1 \, \partial R/\partial Y$ is assumed to be smaller than R, $\partial P_1/\partial Y$ given by equation (19) is also negative.

This negative stiffness is counteracted by the positive stiffness of the trunk tension. If the positive stiffness is more than the negative stiffness, the system is stable. If however, the reverse is true, the system is unstable and the trunk bottom experiences a downward displacement.

The magnitudes of the positive and the negative stiffness change as the ACLS parameters, such as load, are changed. As an

example, Figure 12(a) shows possible values of the two stiffnesses for the prototype trunk at FMA which showed flutter in the 100 to 250 lb load region.
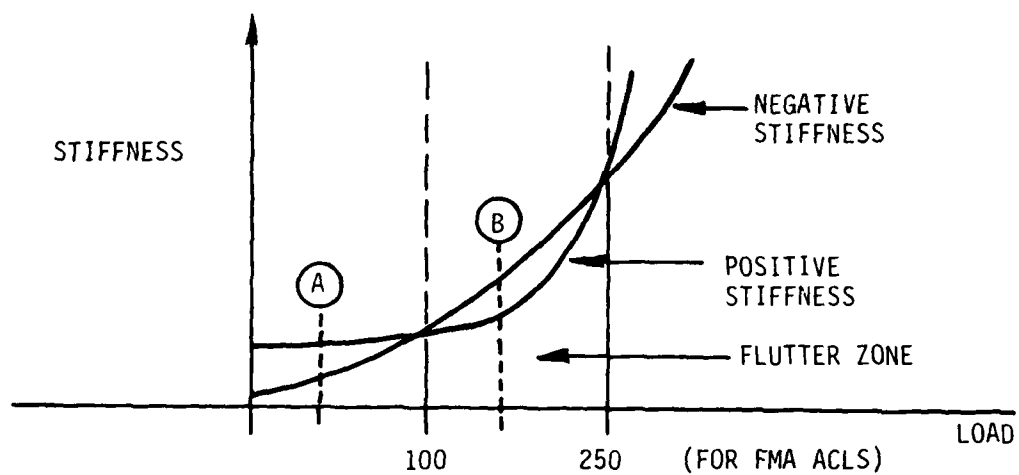
Figure 12(b) shows the trunk motion for cases A and B identified in Figure 12(a). For case A, a small perturbation makes the trunk go in a damped convergent oscillation and no flutter is observed. For case B, however, the equation of motion of the trunk is for an undamped oscillator; which means that an initial perturbation to the trunk bottom would grow causing the trunk to move downwards until one of the following two events occur:

a.   The positive force increases (due to increase in the angle of the tension force when the trunk moves downwards) until it is larger than the negative force, thereby causing the trunk to start moving upwards toward the original position.

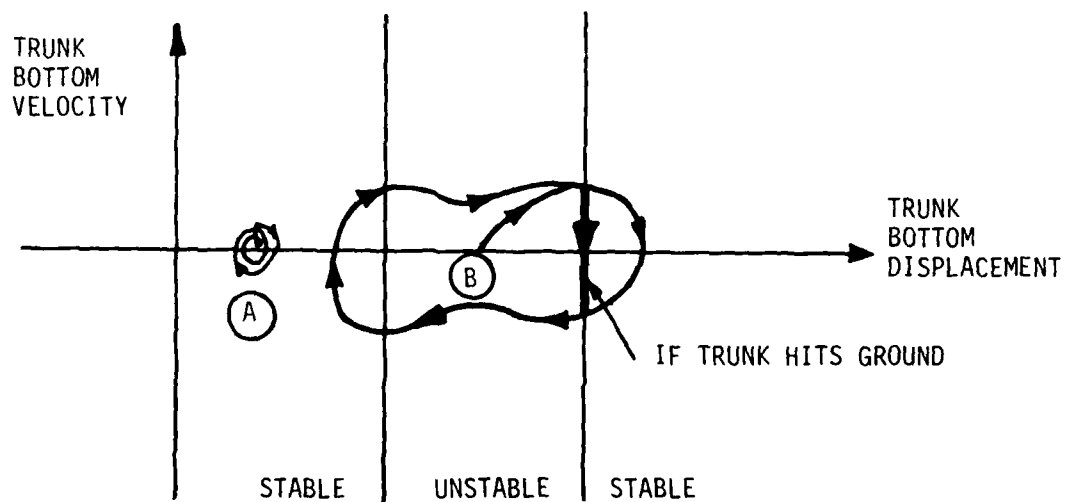b.   The trunk hits the ground before the above happens.

In either case the trunk bottom reverses its direction of motion and starts moving upwards. However, the system becomes unstable once more as it enters the zone where the negative stiffness is larger than the positive stiffness. Therefore, the trunk bottom continues moving upwards until it has moved far enough from the ground so that the negative force becomes smaller than the positive force and the trunk starts heading towards the original position once more. This way a limit cycle motion is created.

To summarize, the trunk bottom executes a limit cycle behavior (that is, it flutters) if

a.   The initial position lies in an unstable zone

b.   The trunk motion resulting from such instability leads to a stable zone.

32

STIFFNESS

NEGATIVE STIFFNESS

POSITIVE STIFFNESS

FLUTTER ZONE

Ⓐ

Ⓑ

100   250   (FOR FMA ACLS)

LOAD

A.   COMPARISON OF POSITIVE AND NEGATIVE STIFFNESS

TRUNK BOTTOM VELOCITY

TRUNK BOTTOM DISPLACEMENT

IF TRUNK HITS GROUND

Ⓐ

Ⓑ

STABLE   UNSTABLE   STABLE

B.   THE LIMIT CYCLE BEHAVIOR

Figure 12.   Possible Mechanism of Instability.

33

An initial qualtitative verification of the flutter model can be made by checking if the model can predict the parametric effects identified in Table 2.

When the brakes are applied, the flutter tendency reduces. The model will predict this because h_1 increases and, therefore, the negative stiffness given by equation (9) or (19) reduces, thereby increasing stability.

Wind can change the flow separation point and thereby affect the flutter stability.

The strakes will bring the separation point closer to the ground. Therefore, h_2 will reduce and the flutter stability will increase as shown by equation (9). Alternatively θ will reduce and therefore $(1 - \cos \theta)$ will reduce, increasing the flutter stability as shown by equation (19).

On rough terrain, h_1 increases, thereby increasing stability.

C.G. location similarily changes h_1, therefore, the stability can change.

Adding inertial dampers will not change the negative stiffness effect of the flow or the positive stiffness due to the tension in the trunk. Therefore, the flutter will not be eliminated. However, for the same force, lateral acceleration of some parts of the trunk will reduce, thereby reducing the flutter amplitude.

If the cushion pressure is increased the negative stiffness will increase as given by either equation (9) or (19), leading to a maximum flutter prone configuration. This matches with one of the conclusions by Forzono (8). The increase in the trunk pressure should increase the trunk tension and thereby the

34

positive stiffness. The flutter stability should then improve. However, increasing the trunk pressure may be accompanied by a corresponding change in some other variables, such as the gap area, which reduce the stability. Also, the instability caused by the negative spring constant only initiates the limit cycle behavior. Once initiated, the amplitude of the limit cycle will depend on location of the stability boundary and the magnitude of the positive stiffness in the stable region.

3.3 Variations in the Basic Model

Although the basic model described earlier is valid for understanding stability of the system, several improvements are needed in order to predict the flutter characteristics more accurately. Such improvements in the model discussed in this section are:

a.   Fan-trunk-cushion flow dynamics

b.   Flexural stiffness and damping of the trunk

c.   Flow from the trunk orifices (at the bottom of the trunk).

Some of the other parameters have not been considered in the model because of a variety of reasons.

The flexural damping of the trunk, although included in the model, is assumed to be zero in the simulations. This is because the initiation of flutter depends on the comparative values of the positive and the negative stiffnesses. Although the flexural stiffness affects the positive stiffness, flexural damping does not. And since the primary objective of the computer program is to study the inception of flutter, the value of flexural damping is assumed to be zero.

The effect of wind on flutter is difficult to model. Assuming that wind can raise the separation point and thereby induce flutter in the trunk, a compensation in the form of a higher separation point in the simulation can be provided while studying a particular trunk design.

Vortex shedding is not incorporated in the model because its effect on the trunk is expected to be negligible.

Effects of the vehicle attitude and the daylight clearance between the ground and the trunk are taken into account by the hard surface clearance to be specified in the model. The weight of the vehicle can be converted to the hard surface clearance, cushion pressure, and trunk pressure for a given design using the computer program developed by FMA (11). Finally, the trunk-ground friction coefficient is not included in the model because the trunk-ground contact is expected to be in the vertical direction, and hence the friction force may not be significant.

3.3.1 Fan-Trunk-Cushion Flow Model

The flow model determines the variations in pressures and flows as a function of time. There are two parts to the flow model: The fluid chambers (that is, cushion and trunk), and the fan. The principal assumptions of the flow model are as follows:

a.   The flow through all orifices is one-dimensional and quasistatic, that is, the pressure in the plane of the orifice is uniform, and the unsteady state terms in Bernoulli's equation are small compared to the change in velocity head.

b.   The flow through the orifices is incompressible, that is, the pressure drop is small compraed to the total pressure, and the air density is constant.

c. The pressure and volume changes of the air during expansion and compression in the various fluid chambers are governed by a polytropic relationship, that is, pv^k = constant.

A schematic diagram of the flow model is shown in Figure 13.

<u>Fan</u> - The static fan characteristics are given by a polynomial (see Figure 14).

$$P_{fan} = \alpha_0 + \alpha_1 Q_{fanx} + \alpha_2 Q_{fanx}^2 + \alpha_3 Q_{fanx}^3 + \alpha_4 Q_{fanx}^4 \qquad (20)$$

where α_i = CQi in computer program

(For a dual fan system, as used in the XC-8A, Q_{fanx} is made half the total fan flow since it is assumed each fan has the same characteristics.)

In dynamic situations the fan characteristics can be modeled by adding inertance of the fan air and the duct air (<u>12</u>). In that case,

$$\frac{d}{dt} Q_{fan} = \frac{P_{fan} - P_t}{I_{fan}} \qquad (21)$$

where, I_{fan} is the inertance of air in the fan and in the duct.
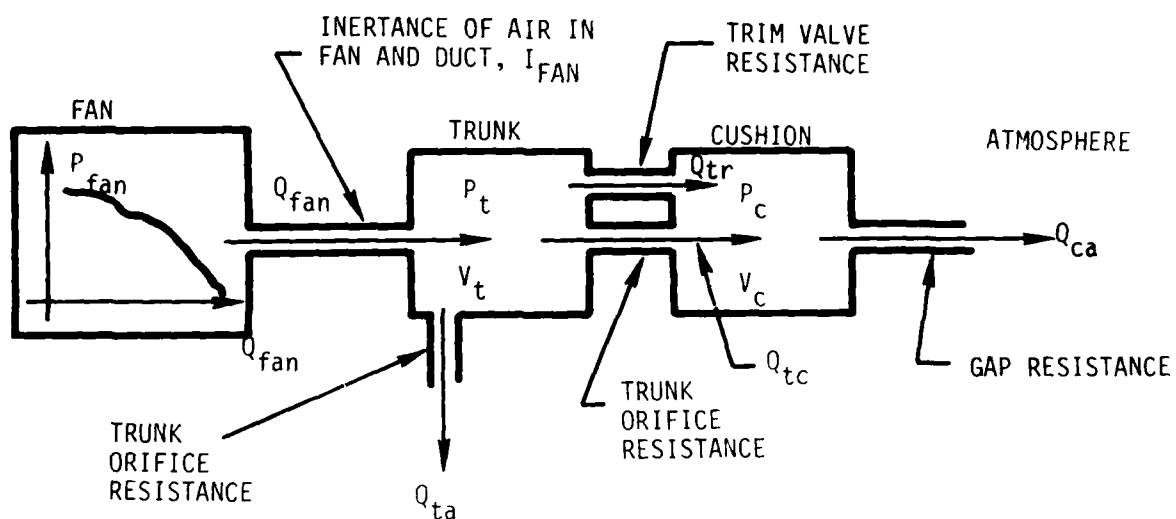
Figure 13. Dynamic Fluid Model

$$P_{fan} = \alpha_0 + \alpha_1 \, Q_{fan} + \alpha_2 \, Q_{fan}^2 + \alpha_3 \, Q_{fan}^3 + \alpha_4 \, Q_{fan}^4$$
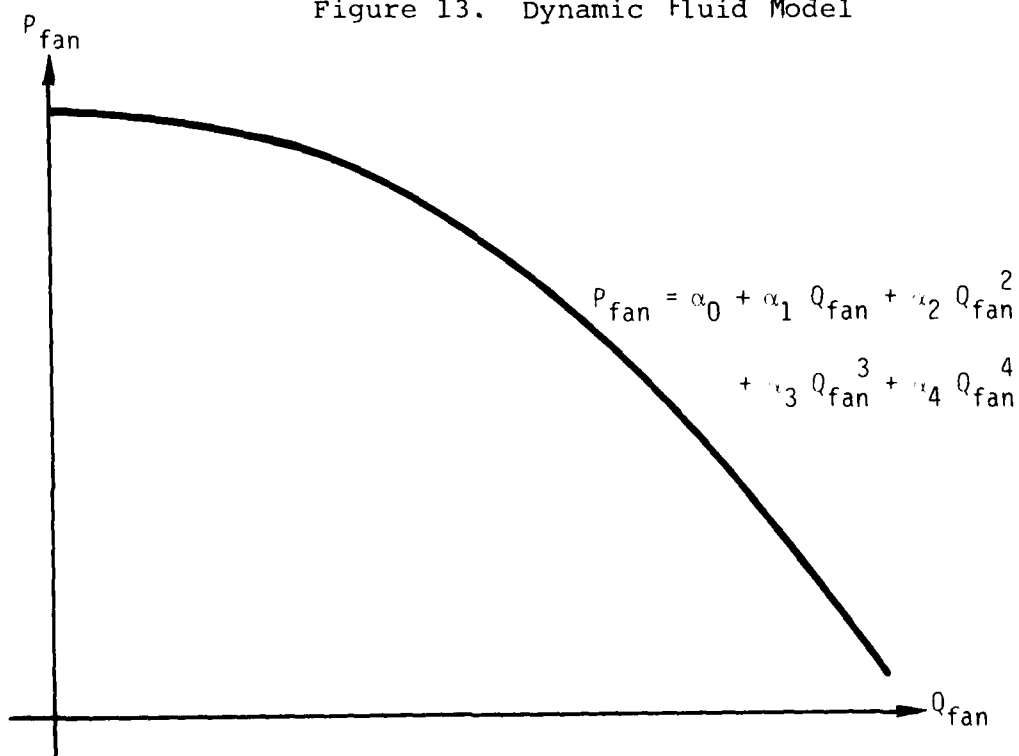
Figure 14. Fan Pressure versus Flow Polynomial.

Trunk - From the polytropic pressure-density relation:

$$\frac{(P_t + P_a)}{\rho^k} = \text{constant} \qquad (22)$$

where ρ = density in slugs/ft^3

Taking the time derivatives,

$$\frac{d\, P_t}{dt} = \frac{k(P_t + P_a)}{\rho} \cdot \frac{d\rho}{dt} \qquad (23)$$

However, conservation of mass in the plenum requires that,

$$\frac{d}{dt}\,(\rho\, V_t) = V_t\,\frac{d\rho}{dt} = \rho\, Q_{fan} - \rho\, Q_{tr}$$

$$- \rho\, Q_{tc} - \rho\, Q_{ta} \qquad (24)$$

(Assuming V_t remains constant during flutter.)

Where

$$Q_{tr} = C_{tr}\, A_{tr}\, \sqrt{\frac{2(P_t - P_c)}{\rho}} \qquad (25)$$

$$Q_{tc} = C_{tc}\, A_{tc}\, \sqrt{\frac{2(P_t - P_c)}{\rho}} \qquad (26)$$

$$Q_{ta} = C_{ta} A_{ta} \sqrt{\frac{2 P_t}{\rho}} \qquad (27)$$

and the variables are defined in the nomenclature.

From equations (23) and (24),

$$\frac{d}{dt} P_t = \frac{k(P_t + P_a)}{V_t} (Q_{fan} - Q_{tr} - Q_{tc} - Q_{ta}) \qquad (28)$$

Similarly

$$\frac{d}{dt} P_c = \frac{k(P_c + P_a)}{V_c} (Q_{tr} + Q_{tc} - Q_{ca}) \qquad (29)$$

where

$$Q_{ca} = v_1 h_1 L_t$$

and

v_1 = gap velocity

h_1 = gap height

L_t = total gap width.

Equations (20), (21), (28) and (29) represent the fluid flow model. Equation (28) gets modified when the trunk flow

40

model is considered. In that case the flows Q_{tc} and Q_{ta} do not include air going to the trunk bottom zone which is calculated separately. Similarly Q_{ca} is modified so that it represents the flow from only the cushion and does not include the flow from the orifices located on the inside part of the trunk.

3.3.2 Flexural Stiffness and Damping of the Trunk

The flexural stiffness of the trunk is taken into account by assuming a linear relationship between the torque required to bend a strip of 1 ft wide, ℓ ft long and the angle of bending. This equation can also be derived if the trunk behavior is assumed to be similar to that of an elastic beam [see Roark for example (13)].

For the beam shown in Figure 15,

$$R = \frac{EI}{\tau_K} \tag{30}$$

but

$$R = \frac{\ell}{\theta} \tag{31}$$

therefore

$$\frac{\tau_K}{\theta} = \frac{EI}{\ell} \tag{32}$$

41
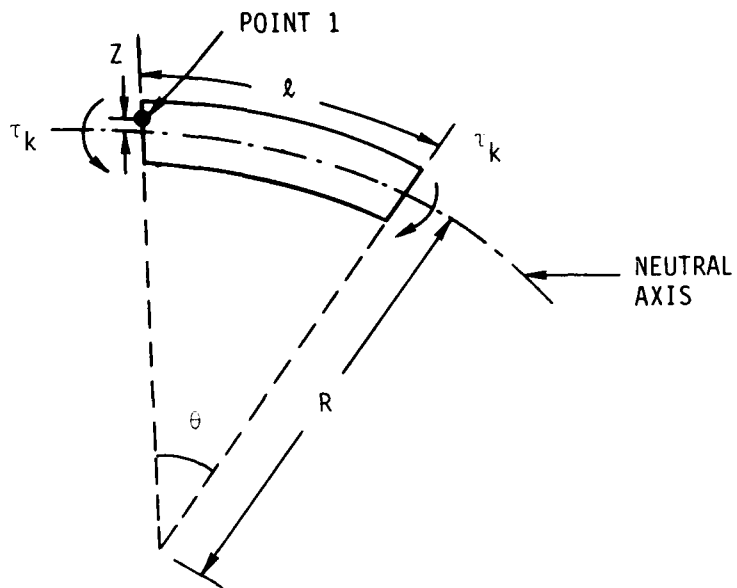
Figure 15. Bending of an Elastic Beam.

$$\tau_K = \frac{EI}{\rho} \theta \qquad (33)$$

or

$$\tau_K = \frac{K_\ell}{\ell} \theta$$

where

K_ℓ = flexural stiffness of the trunk material per unit width per unit length

The flexural stiffness for a particular trunk can easily be estimated from equation (33) where E is obtained from material stiffness (in stretch) and I is given by,

$$I = \frac{1}{12} bd^3 \qquad (34)$$

where

b = width of the 2-D trunk cross section (equals 1 ft)

d = thickness of the trunk material (stretched).

A similar relationship between the damping torque and the bending rate can be derived. Consider once again the beam shown in Figure 15.

The stress in the beam is given by,

$$\sigma = \frac{MZ}{I} \qquad (35)$$

where

M = includes the torque due to flexural stiffness and due to flexural damping

Z = distance from the neutral axis of Point 1 in Figure 15

σ = the tension (or compression) stress at that point.

The strain at that point is given by

$$\varepsilon = \frac{\Delta \ell}{\ell} = \frac{Z\theta}{\ell}$$

(36)

If the material damping is present, the stress in equation (35) can be assumed to be related to the strain through the following equation.

$$\sigma = B\dot{\varepsilon} + E\varepsilon$$

(37)

This relationship is based on behavior of material under cyclic stress as shown in Figure 16. From equations (35), (36), and (37).
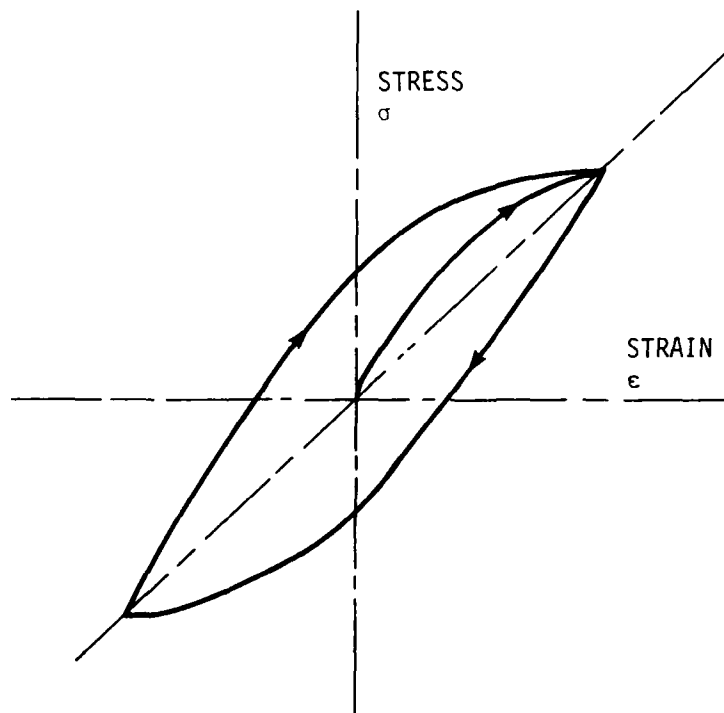
Figure 16. The Stress-Strain Relationship for the Trunk Material (Reference 14, Chapter 14).

44

$$\sigma \quad \text{due to bending rate} \quad = \quad \frac{BZ}{\ell}\,\dot{\theta} \tag{38}$$

$$M \quad \text{due to bending rate} \quad = \quad \tau_B \quad = \quad \frac{BI}{\ell}\,\dot{\theta} \tag{39}$$

or

$$\tau_B \quad = \quad \frac{B_\ell}{\ell}\,\dot{\theta} \tag{40}$$

where

B_ℓ = flexural damping of the trunk material per unit width per unit length.

The relationships expressed in equations (33) and (40) can be taken into account in the lumped mass trunk model by determining equivalent forces acting on the trunk masses shown in Figure 17. For such a case ℓ in equations (33) and (40) is mean of lengths ℓ_1 and ℓ_2, whereas the forces F_1 and F_2 are given by:

$$F_1 \quad = \quad \frac{\tau_B - \tau_K}{\ell_1} \tag{41}$$

$$F_2 \quad = \quad \frac{\tau_B - \tau_K}{\ell_2} \tag{42}$$

45
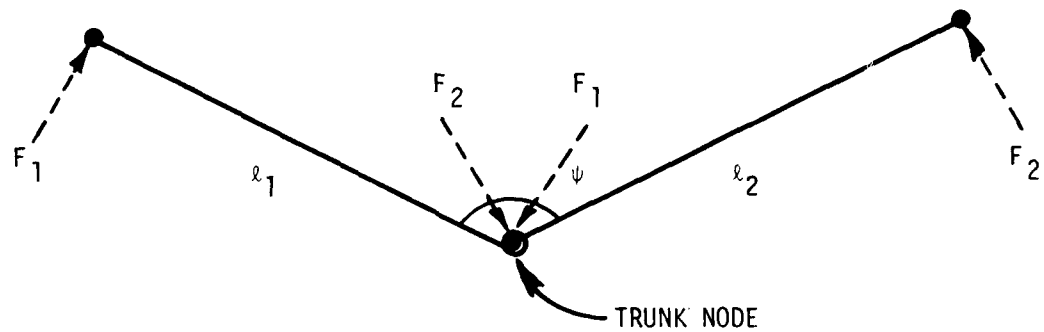
Figure 17.   Flexural Stiffness Model.

where

$$\tau_K = \frac{K_\ell}{\ell} (\psi' - \psi)$$

$$\tau_B = \frac{B_\ell}{\ell} \dot{\psi}$$

and

$$\psi' = \text{initial angle.}$$

46

3.3.3 Flow from the Trunk Orifices

So far the effect of the flow from the trunk orifices at the bottom of the trunk has been assumed to be negligible. In order to improve accuracy of the simulation this effect can be included by considering the continuity and the momentum equations for the flow at the bottom of the trunk.

Consider a control volume as shown in Figure 18. This control volume is located on the outer side (atmosphere side) of the trunk, but the equations derived would be valid for a control volume located on the inner side also. The mass rate of flow, velocity of flow, pressure and the flow area on entrance and exit of the control volume are as shown in the figure. Flow dw_ℓ represents the trunk orifice flow per unit width entering the control volume.

In order to apply the momentum equation we should find out the forces acting on it as shown in Figure 19. In this figure, force PA_ℓ is exerted by the trunk on the control volume whereas PA and $(P + dP)(A + dA)$ are forces exerted by the fluid pressure.

From force balance in x direction:

$$\text{Total Force in } x \text{ direction} = F_x = PA$$

$$- (P + dP)(A + dA)$$

$$+ PdA_\ell \sin \phi \qquad (43)$$

$$\text{However, } dA_\ell \sin \phi = dA \qquad (44)$$

47
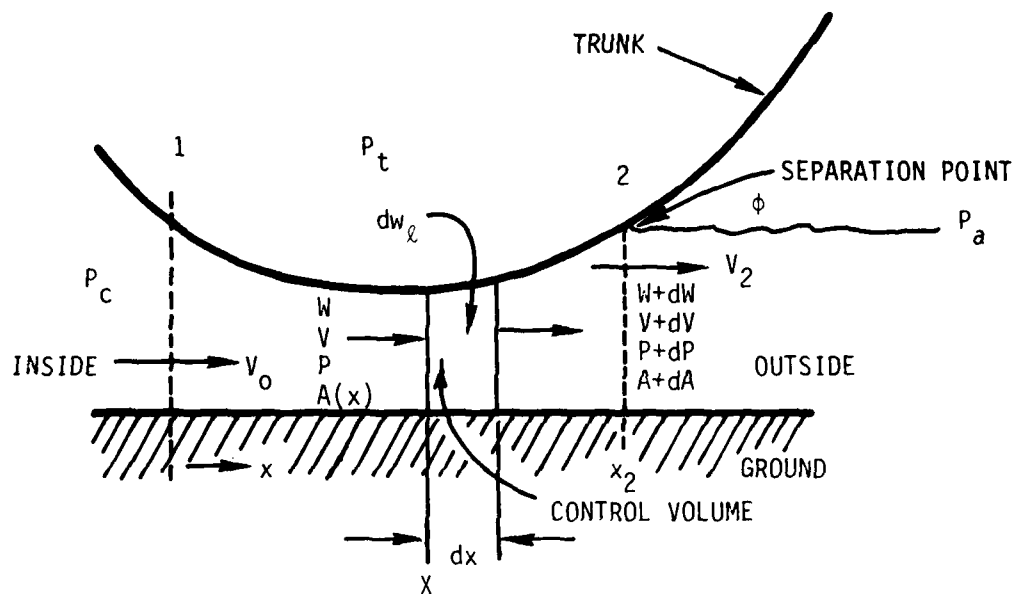
W = MASS RATE OF FLOW

V = FLOW VELOCITY

P = PRESSURE

A = AREA

W_ℓ = TRUNK ORIFICE FLOW

X = DISTANCE

Figure 18. Trunk Orifice Flow Model.
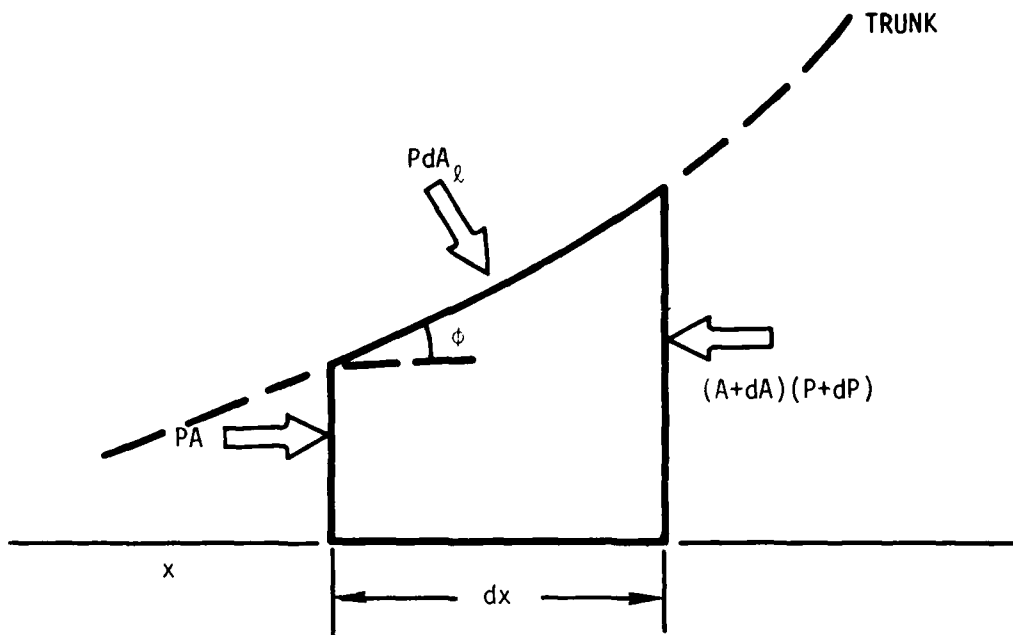
Figure 19.   Force Balance of the Control Volume.

Therefore

$$F_x = PA - (P + dP)(A + dA) + PdA$$

$$= -AdP \qquad (45)$$

However, from the momentum equation

$$F_x = -AdP = (w + dw)(v + dv) - vw \qquad (46)$$

which leads to

$$-AdP = wdv + vdw \qquad (47)$$

49

but

$$w = v\rho A$$

therefore

$$-AdP = v\rho A dv + v dw \qquad (48)$$

and

$$-dP = v\rho dv + \frac{v}{A} dw \qquad (49)$$

Integrating from the cushion cavity to the control volume:

$$- \int dP = \rho \int v dv + \int \frac{v}{A} dw \qquad (50)$$

$$(P_c - P) = \frac{\rho}{2} \left(v^2 - v_0^2 \right) + \int_0^x \frac{v dw}{A} \qquad (51)$$

$(v_0 \quad 0,$ as assumed earlier$)$

Similarly integrating equation (50) from the cushion cavity to the atmosphere

$$P_c - P_a = \frac{\rho}{2} \left(v_2^2 - v_0^2 \right) + \int_0^{x_2} \frac{v}{A} dw \qquad (52)$$

The integral term $\int_0^x v/A\, dw$ can be evaluated by applying the continuity equation to the control volume in Figure 18.

$$w - (w + dw) + dw_\ell = 0 \tag{53}$$

therefore

$$dw = dw_\ell \tag{54}$$

where

dw_ℓ is obtained from orifice equation

$$dw = dw_\ell = dA_0 C_d \sqrt{\frac{2}{\rho}(P_t - P)} \quad \rho \tag{55}$$

where

dA_0 = the trunk orifice area in control of the volume

C_d = the trunk orifice discharge coefficient

Substituting the value of dw thus obtained in equation (51), we get:

51

$$P_c - P = \frac{\rho}{2}\left(v^2 - v_0^2\right)$$

$$+ \int_0^x \frac{v}{A} C_d \sqrt{\frac{2}{\rho}(P_t - P)} \; dA_0 \, \rho \qquad (56)$$

This equation in conjunction with equation (52) can be employed in an iterative procedure to obtain values of pressure, P, and velocity, v, under the trunk (1). This pressure, P, represents the pressure obtained using Bernoulli's equation in the basic model while considering forces on the trunk.

4. MODEL VERIFICATION

In order to demonstrate validity of the model, the flutter observed in the XC-8A trunk is simulated using a computer program developed based on the model (see Reference 1 for details on the computer program). The parameters assumed in the simulation are summarized in Table 3 and Figures 20 and 21. In addition, the simulation assumes that only the sides of the trunks experienced flutter* and the separation angle is 12 deg.**

The simulation includes:

- Characteristics of the air source
- Dynamics of the cushion air
- Dynamics of the trunk air
- Trim valve flow
- Trunk orifice flow
- Trunk characteristics (size, mass, elasticity).

The test selected for simulation is S-020877-1 for the following two reasons:

- Data are available in great detail
- Film of the test is available.

This test was performed on a trunk configuration incorporating a tape-restraint system inside the front lobe of the trunk. However, the restraint system failed to prevent occurrence of flutter. Therefore, these data could probably be treated as those on an unmodified trunk.

---

*Based on the flutter observations from the XC-8A film and the film supplement to this report.

**Based on the preliminary tests described in Appendix A.

53

TABLE 3. PRINCIPAL XC-8A TRUNK PARAMETERS

General	
Trunk type	XC-8A, Trunk No. 3
Average trunk material density	0.84 lb/ft^2
Trunk girth (inflated at 330 psfg)	12 ft
Horizontal distance between attachments	4.725 ft
Vertical distance between attachments	1.272 ft
Trunk elasticity per unit width (See Figure 20)	3926 lb/ft
Trunk volume	1041 ft^3
Cushion Volume	245 ft^3
Trunk Orifices	
Number of rows	14
Number of orifices per row	484
Distance between rows	0.25 ft
Distance between first row and inner attachment point	2.5 ft
Effective orifice area	0.0546 in.^{2}
Number of trim valves open	15
Fan Characteristics	
As shown in Figure 21	
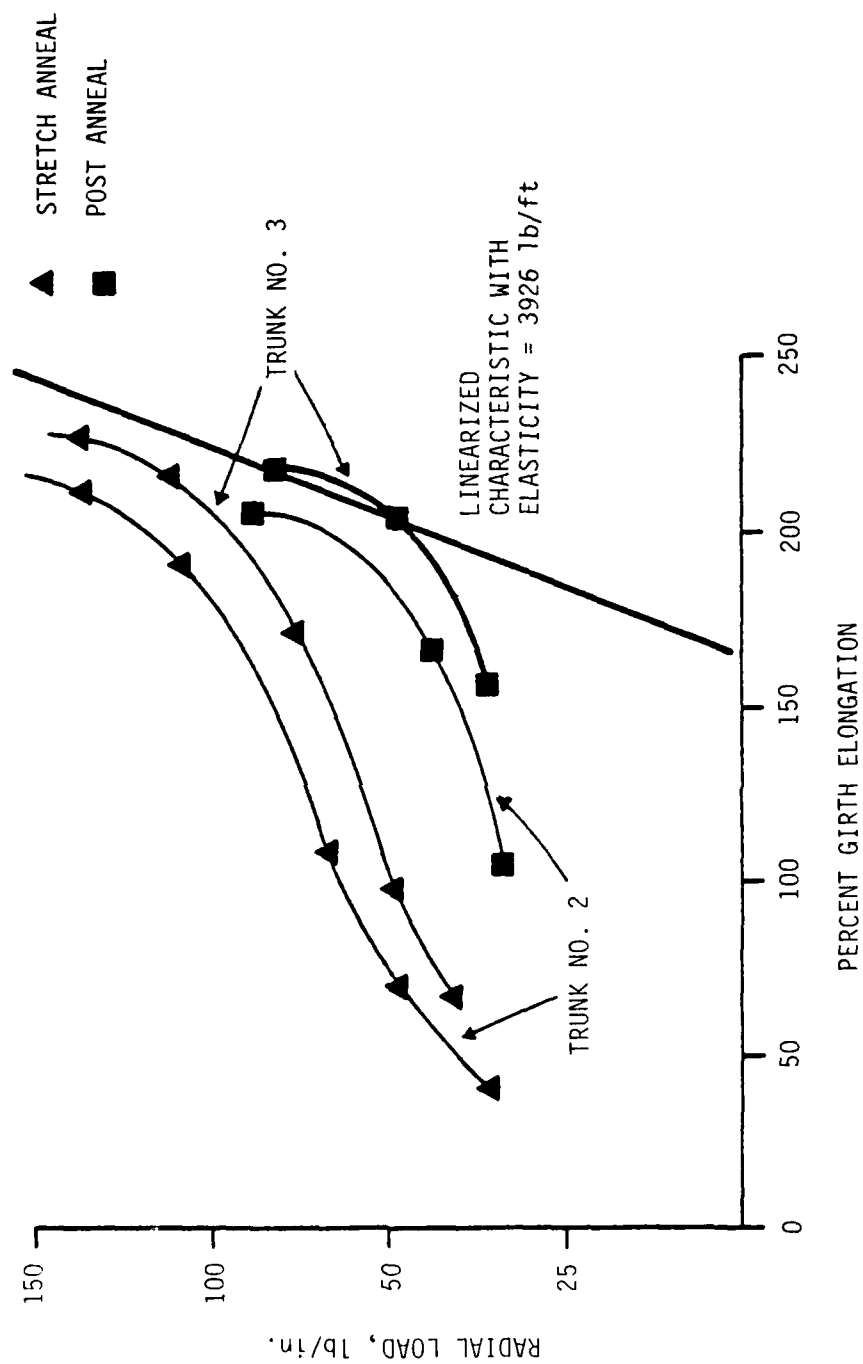
Figure 20. Radial Load versus Girth Elongation of XC-8A Trunk.

55

Figure 21. The XC-8A Fan Characteristics.

56

The relevant part of the log of events for the test is shown in Figure 22 and the corresponding performance parameters are in Figure 23. Finally Figure 24 shows digitized values of the various pressures and flows for two selected cases. Of these cases, case 1 corresponded to absence of flutter due to brakes on and case 2 showed flutter with brakes off.

The results of the simulation runs corresponding to these cases are shown in Table 4.* As shown in the table, the computer program succeeds not only in predicting the occurrence of flutter but also in predicting the relevant parameters correctly.

In addition to the table, the simulation results are presented in Figures 25 through 31. In these results the trunk motion is represented in terms of vertical motions of several lumped mass nodes, the location of which is shown in Figure 25. The vertical displacement of nodes 8 and 9 located on the trunk bottom is shown in Figure 26 for case 1. As can be seen from the figure the nodes show no motion. The corresponding variations in the trunk and the cushion pressures are shown in Figure 27 and those for the total flow and the trunk orifice flow are in Figure 28.

For the case when the flutter is present, Figures 29 through 31 show variations in the node location, pressures and flows. As shown in Figure 29 the trunk bottom exhibits a flutter at 28 Hz frequency which matches well with the 20 Hz reported for XC-8A (5). Also the in-phase motion of the nodes indicate that the trunk bottom executes a "plate-like" motion which is verified by the XC-8A film and the film supplement to this report. The amplitude of the flutter is predicted to be about 3/4 in. which may be lower than that observed. However from the XC-8A film it is difficult to determine what the actual flutter amplitude is.

---

*Case 1 is simulated by introducing 0.1 ft minimum gap which would be the result of braking.

S-020877-1

TIME (?)	EVENT
1320.00	ATL
2138	IDLE — NO TORQUE INDICATIONS LEFT ASP-10
152746	STOP
133448	IDLE LT
134013	IDLE
134253	RUN — DUAL ASP-10 * 15 TRIM PORTS
Case 1 [134459	P_T → 335 — Film Sequence Letters
134620	TAPE ON BL ON P_T 330
2 [134707	B OFF FLUTTER (A) Aft of 90°
134726	Slight heave — P_C slight oscillation
	slight rolling
135040	P_T ↓ 307 start
135049	P_T 320
135330	P_T 307 slight flutter inside of heave
135402	B off (B) flutter
135433	DIFFUSER str 260 left
135515	P_T ↓ 286 psi
135653	B off (C)
135736	roll A/C
135813	B ON stop flutter
	P_T 265
	P_T ↑ 298
140055	P_T ↑ 323
	B ON flutter stop
40153	B OFF

Figure 22. Log of Events for the S-020877-1 Test.

TEST # S-020877-1

ITEM-6 219

SNO/ICE on

D.C. PERFORMANCE PARAMETERS

TIME	Nc	Ncr	Tgl	Tgr	Ngbot	Ngl	Ngr	TGTl	TGTr	Qol	Qor	P7	Pe
133116	85.3	85.1	50.5	49.5	91	91.5	93.5	790	800	92	91	229	89
134835	85.2	84.0	50	48	91.0	92.8	93.5	795	760	92	89	330	135
135121	81.5	79.9	46	44	88.5	91.4	91.9	790	750	88	82	307	130
135537	77.5	74.5	42	40	86.5	90	92.5	800	790	82	79	205	130
135913	73.1	71.5	57	35.5	83.0	83.8	84.5	790	740	78	77	240	125
140324	80	78.5	41	41	88.8	91.5	91.9	820	710	82	78	328	80
140516	76	75	42	40	86.0	90	92.2	800	760	80	77	307	75
140810	73.3	71.4	39	37	83.8	88.1	89	795	750	78	75	296	70
141031	70.2	66.5	36	34	82.0	87	87	760	740	70	65	265	65
141515	87.2	84.9	44	46	91.4	92.2	92.4	830	790	100	92	307	105
141707	84.1	81.5	46	44	86.4	92	92	825	795	95	89	265	110
141920	80	77.5	42.1	36.1	82.0	90.5	90.7	810	755	89	82	265	95
142056	74.5	71.0	42.5	36.5	88.0	90.5	90.7	810	740	88	81	265	135
142?6	-	103	60	60	100.7		100	890	890		122	245	65
144059	100.9	100.9	58	58	98.8		98.8		860		120	286	50
144316	93.5	93.5	51	51	94.8		66		810		110	265	45

Case 1 →

2 →

Figure 23. The Performance Parameters for the S-020877-1 Test.

Figure 24. Digitized Instrumentation Output S-020877-1 Test.

Case 1

Figure 24. Digitized Instrumentation Output S-020877-1 Test (Continued)

61

TABLE 4. VERIFICATION OF FLUTTER PROGRAM

Case		Hard Surface Clearance	Trunk Pressure psfg	Cushion Pressure psfg	Total Flow ft^3/sec	Flutter
1	Experiment*	?	335	89	1456	No
	Simulation	2.775†	292	80	1520	No
2	Experiment**	?	330	135	1439	Yes
	Simulation	2.775	310	130 (mean)	1485	Yes

*Trig time 134346-134454, test S-020877-1
**Trig time 134707-134835, test S-020877-1
†With an 0.1 ft minimum gap to simulate brakes. Simulation runs with the hard surface clearance equal to 2.7 and 2.6 ft also showed no flutter.

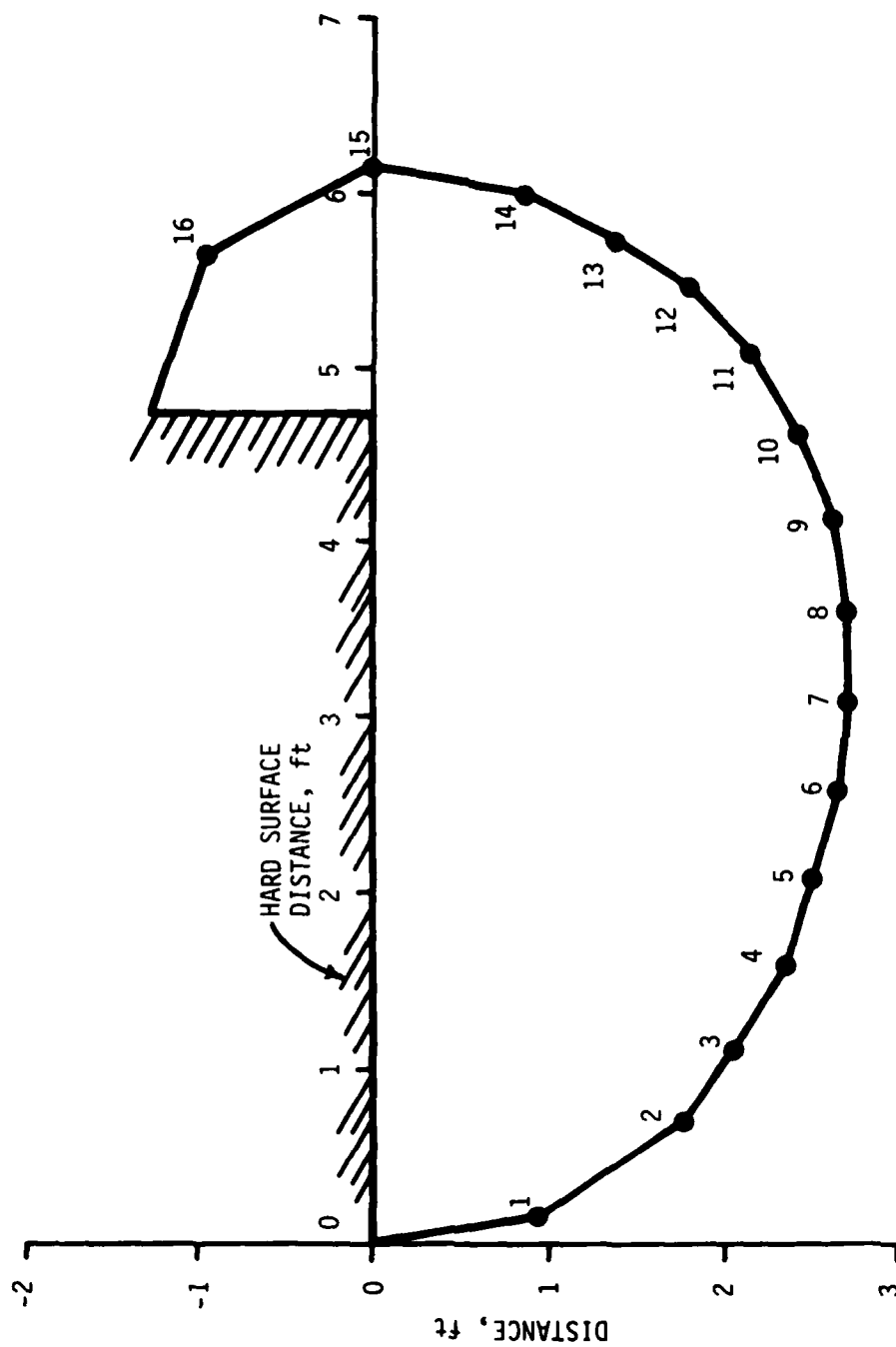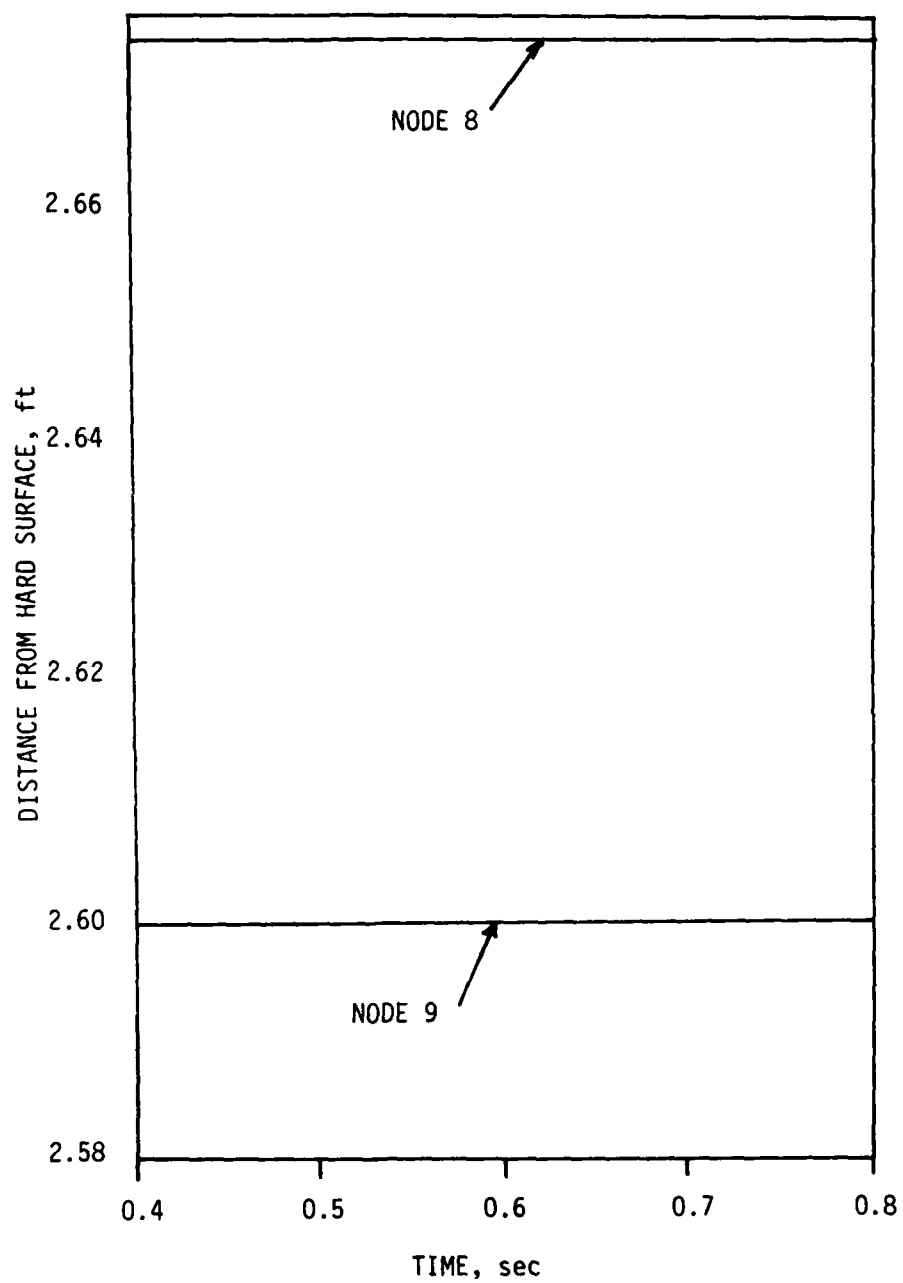Figure 25. Initial Location of Nodes on XC-8A Trunk.

63

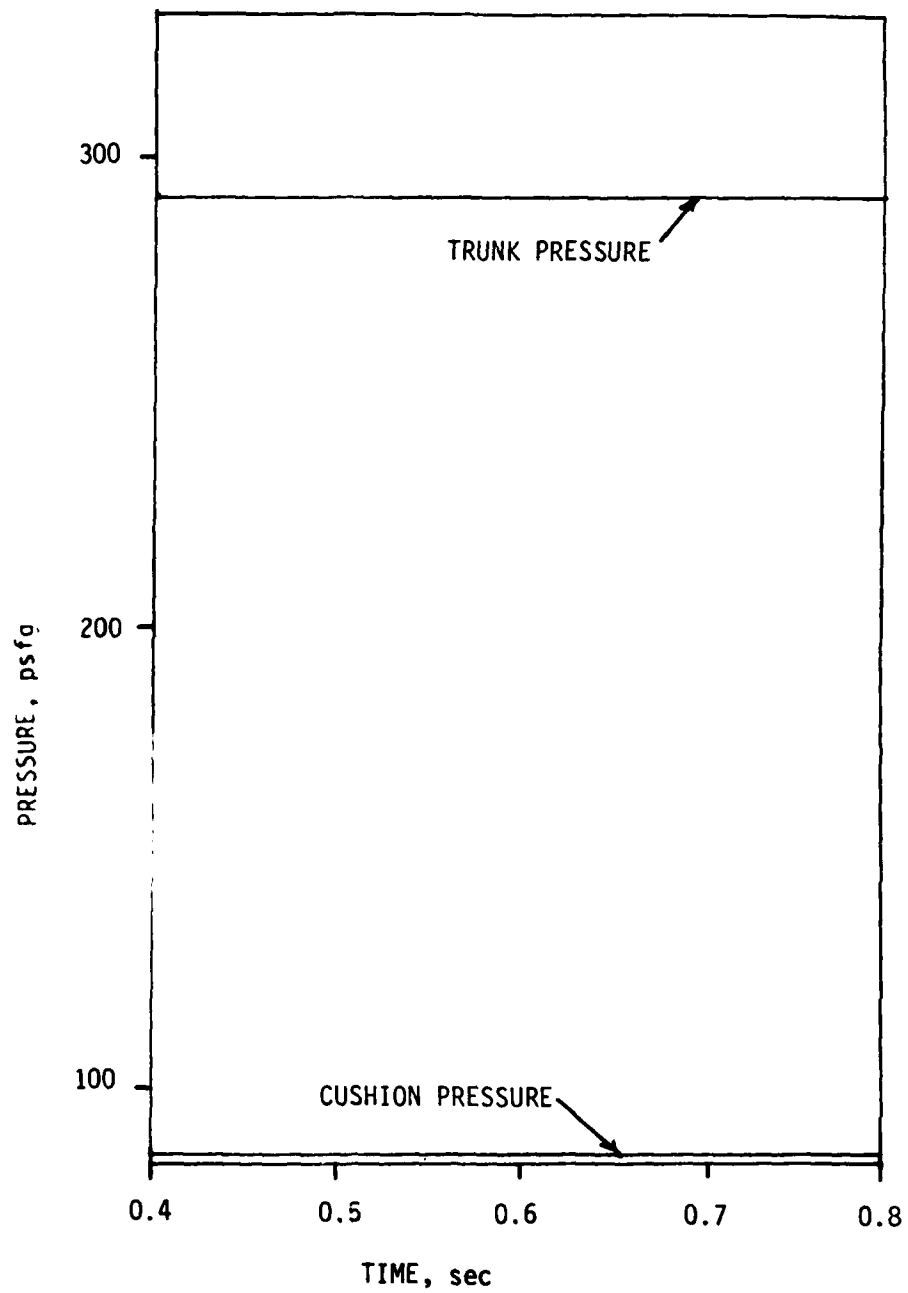Figure 26. Predicted Trunk Motion, Case 1.

Figure 27. Predicted Pressure Variations, Case 1.
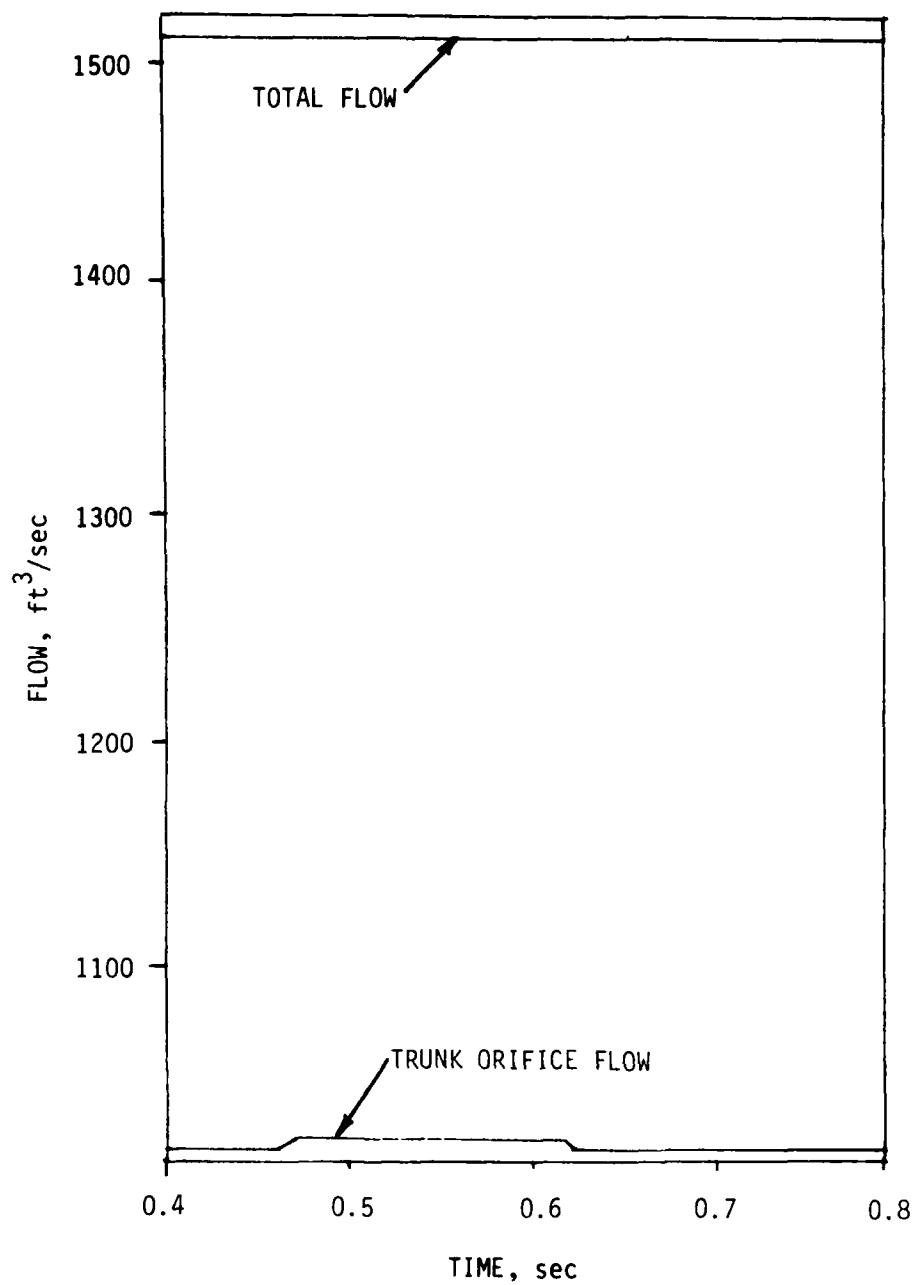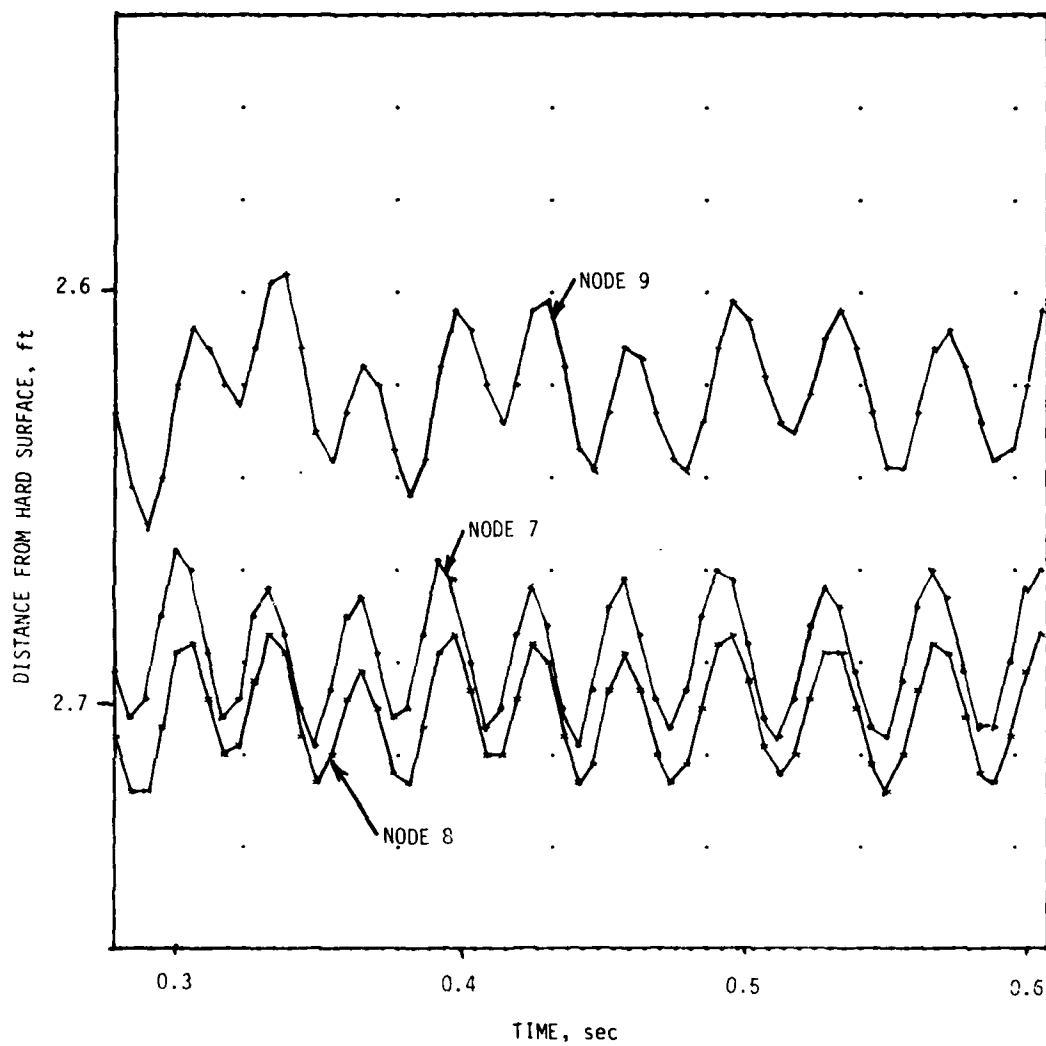
65

Figure 28. Predicted Flow Variations, Case 1.

Figure 29.   Predicted Trunk Motion, Case 2.

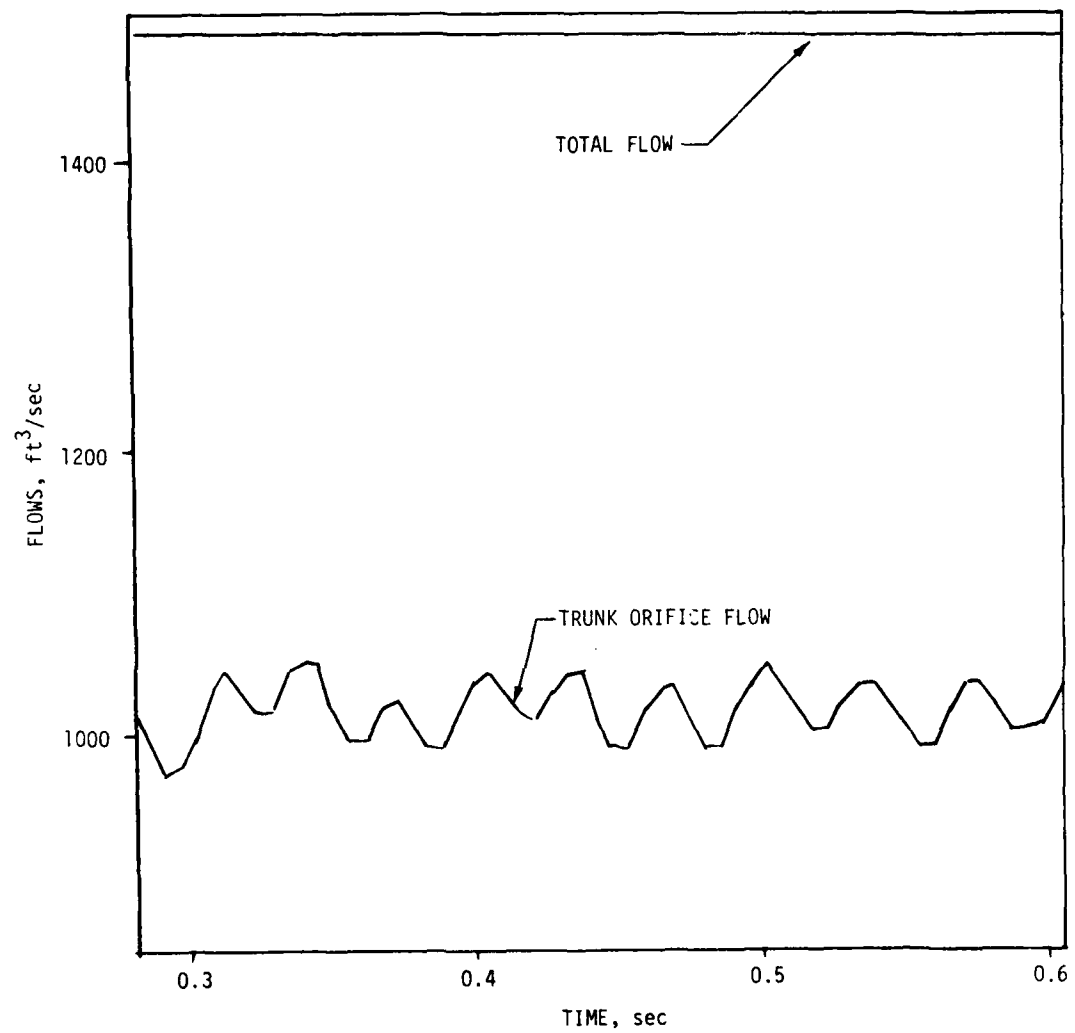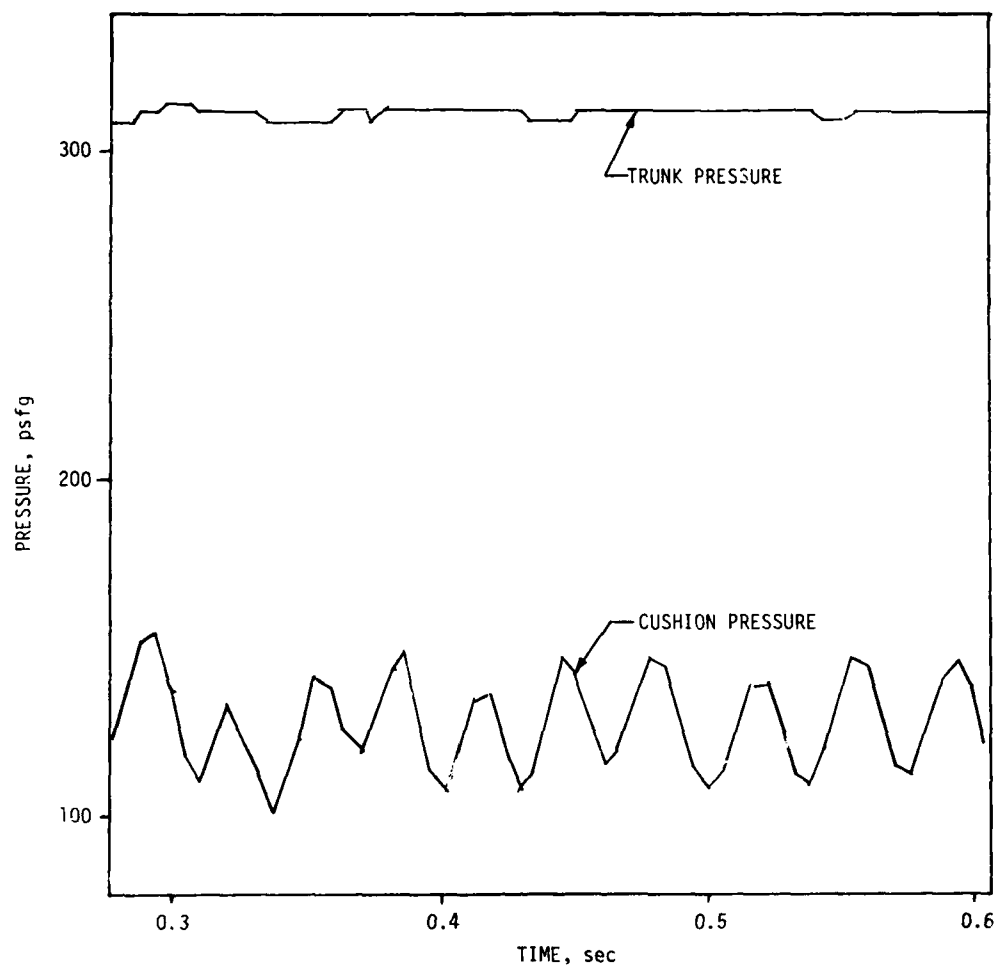Figure 30.   Predicted Pressures, Case 2.

Predicted Flows, Case 2.

The cushion pressure varies about a mean value of 130 psfg, with 28 Hz frequency and about 40 psfg peak-to-peak value. Observing the phase difference in the cushion pressure variations and the node displacements, it seems that the cushion pressure reaches the maximum value just after the trunk is at the lowest point. This is because the outflow from the cushion, reduced due to a reduction in the gap height, is lower than the inflow until the trunk bottom is about halfway between the peaks. The resulting net inflow causes the cushion pressure to rise.

The trunk pressure remains practically constant during flutter, and therefore the total fan flow also does not change. However, the trunk orifice flow varies at the flutter frequency because of the changes in the pressure under the trunk bottom.

The illustrative simulation described in this section demonstrates the ability of the model to predict inception of the flutter and its frequency. The flutter amplitude is perhaps predicted to be lower than that observed, however, with additional investigations suggested in Section 6 the accuracy of the model will increase still further.

With the model verification thus completed, the flutter model is used next to investigate solutions to the flutter problem.

5. FLUTTER SUPPRESSION

Based on the model of the flutter and the experimental results, several ways of reducing or eliminating flutter can be identified as described in this section.

5.1 Methods of Suppressing Flutter

Basically one or both of the following two modifications are required to suppress flutter.

a. Modifying trunk

b. Modifying flow.

In each category a variety of solutions can be proposed as shown in Table 5.

5.1.1 Modifying Trunk

One of the ways of suppressing the flutter through trunk modification involves increasing the stiffness at the bottom of the trunk so that the negative stiffness effect created by the flow can be counteracted, thereby eliminating inception of the flutter. There are two ways of adding this positive stiffness. The tuned "damper," shown in Figure 32, is an extension of a method by which damping is provided in mechanical systems (such as overhead wires, off-shore platforms). In those cases the spring-mass attachment to the vibrating system has a natural frequency identical to that of the system. A resulting out-of-phase motion of the spring-mass attachment adds damping to the system.

71

TABLE 5. PROPOSED WAYS TO ELIMINATING TRUNK FLUTTER

1. Modifying Trunk

    a. Increasing stiffness at bottom

        • Tuned "damper"

        • Internal spring

    b. Increasing flexural stiffness

    c. Increasing hoop tension

        • Circular trunk

    d. Incorporating hybrid trunk

2. Modifying Flow

    a. Lowering separation point

        • Strakes

        • Air strakes

    b. Producing a minimum gap

        • Corrugated trunk

        • Strips

        • Tubes

    c. Changing operating condition

MASS

SPRING
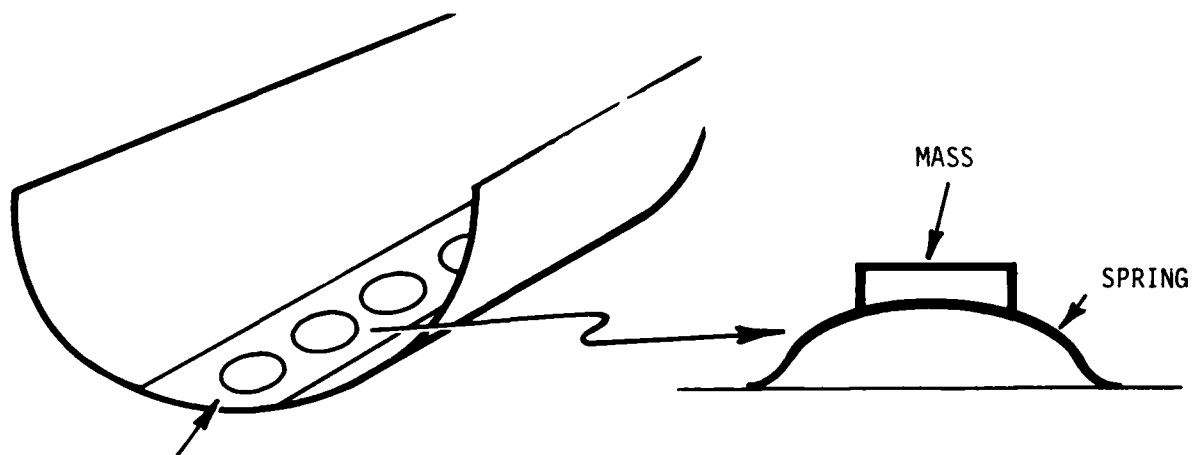
DAMPERS MOUNTED ON THE INSIDE

- IF NATURAL FREQUENCY OF THE DAMPER IS MUCH LESS THAN THAT OF THE FLUTTER THEN IT CAN PROVIDE A POSITIVE STIFFNESS TO COUNTERACT THE NEGATIVE STIFFNESS

- MAKES THE TRUNK HEAVIER

Figure 32.   Flutter Suppression through Tuned Damper.

To suppress flutter, however, additional stiffness is required and not damping. Therefore the spring-mass attachment has a natural frequency much lower than the flutter frequency. This way the mass remains essentially stationary and the stiffness of the spring contributes directly to counteract the negative stiffness due to flow.

Another way of increasing the positive stiffness is through internal spring shown in Figure 33. Here the spring stiffness has to be judiciously selected so that a sufficient additional positive stiffness is provided.

Increasing the flexural stiffness, as shown in Figure 34, also increases the resistance of the trunk to the negative stiffness effect of flow. This concept is demonstrated by a trunk with higher stiffness fabricated by FMA as part of the NASA
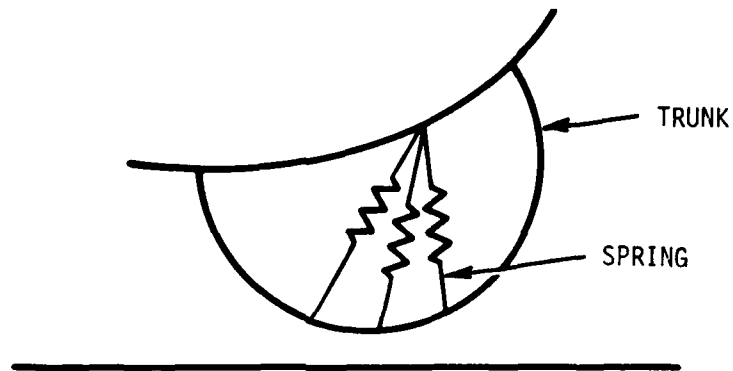
STRETCHED SPRINGS ATTACHED TO THE TRUNK BOTTOM TO
INCREASE THE POSITIVE STIFFNESS

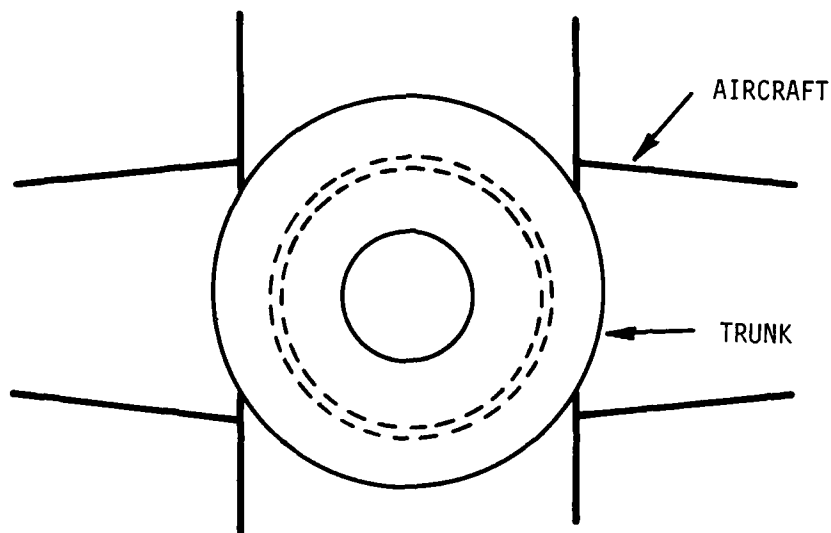Figure 33.   Flutter Suppression through Internal Springs.
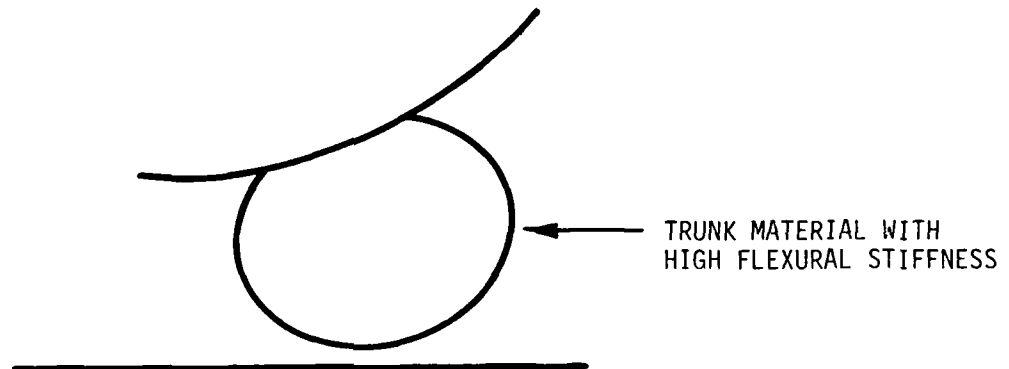
- INCREASES POSITIVE STIFFNESS TO COUNTERACT
  THE NEGATIVE STIFFNESS DUE TO THE AIR FLOW

- LESS RETRACTABLE TRUNK

Figure 34.   Flutter Suppression through Increased Flexural
           Stiffness.

74

contract on ACLS. This trunk, made out of Kevlar coated with polyurethane, did not exhibit flutter even though it had the same dimensions and flow field as the prototype trunk described in Section 2. However, increased weight and reduction in retraction capability may make this option less attractive.

The hoop tension may provide resistance to trunk motion and thereby reduce flutter. One of the problems with the current trunk design is the absence of hoop tension in the trunk sides. If, however, the trunk is made in a doughnut shape, as shown in Figure 35, there will be no parts without hoop tension. This may lead to a more stable design as far as the flutter is concerned.

One way of eliminating flutter which requires significant changes in the ACLS design is to incorporate one of the hybrid trunks shown in Figure 36. The hybrid trunk will be effective
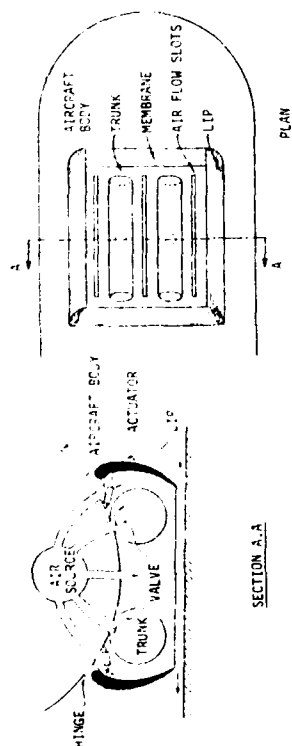

- MAY REDUCE FLUTTER DUE TO ABSENCE OF ANY ZONE WITH NO HOOP TENSION

- DIFFICULT TO ACCOMMODATE ON THE AIRCRAFT FUSELAGE

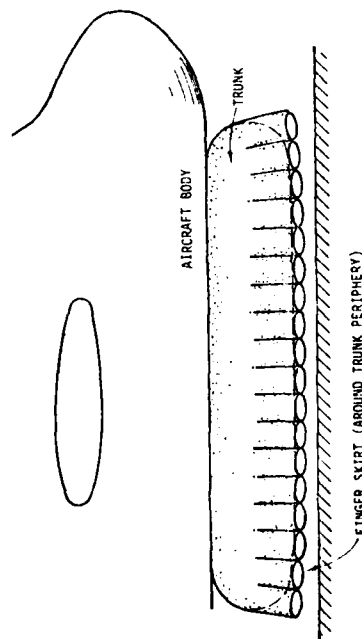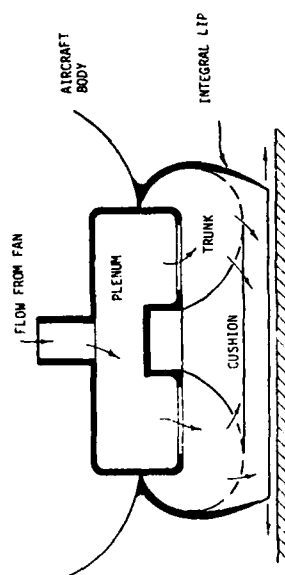Figure 35. Flutter Suppression through Circular Trunk.

75
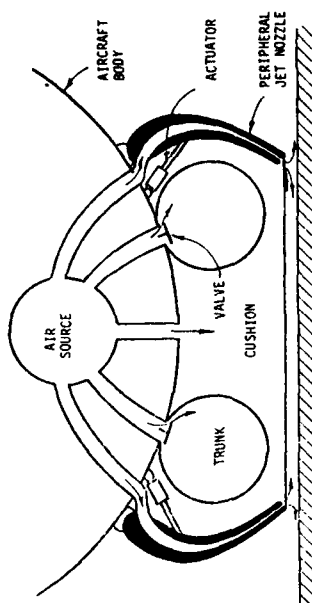
B. TRUNK - PERIPHERAL JET HYBRID SYSTEM

D. INTEGRAL LIP HYBRID SYSTEM

A. TRUNK-LIP HYBRID SYSTEM

C. TRUNK - FINGER SKIRT HYBRID SYSTEM

Figure 36. Flutter Suppression through Hybrid Trunk Designs.

76

because it eliminates a function which the trunk is not ideally suited to perform; that of containing the cushion air. The trunk is a very attractive way of absorbing the initial impact but it does not play the role of a hovercraft skirt very well when the aircraft is taxiing. This is one of the prime causes of problems such as flutter and excessive trunk wear. The hybrid trunk solves the problem by incorporating a hovercraft skirt in addition to the ACLS trunk. The trunk still absorbs the initial impact, but in the taxiing operation the skirt (or lip) takes over the role of containing the cushion air. The advanced technology of hovercraft design will assist greatly in designing a low wear, flutter free skirt.

There may be a variety of configurations for the hybrid trunk as shown in Figure 36. Some of the options may be easier to fabricate (for example, the integral lip hybrid system) than others. The lip can also be designed to serve as a landing gear door, as shown for configurations in Figure 36(a) and (b). Finally, the trunk finger skirt hybrid system shown in Figure 36(c) incorporates the finger skirt which is quite popular among the hovercraft manufacturers.

5.1.2 Modifying Flow

One of the ways in which the flow can be modified is to lower the separation point. As shown by Equation (9) (or (19)), lowering the separation point will reduce the negative stiffness and thereby increase the stability. One possible implementation of this concept is to incorporate strakes which have been tried (5) and proved to be reasonably successful in suppressing flutter. Air strakes shown in Figure 37 may perform the same function but lead to a cleaner configuration which requires additional power.
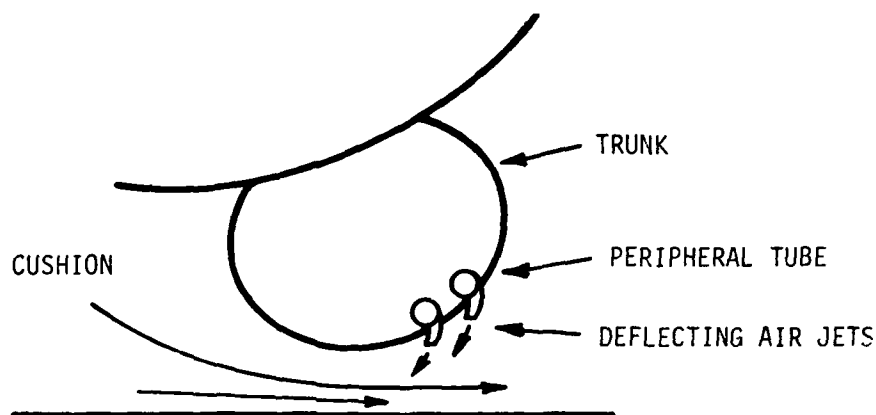
- THE SEPARATION POINT IS MOVED DOWNWARDS TO REDUCE THE NEGATIVE SPRING EFFECT

- INCREASED POWER CONSUMPTION

Figure 37. Flutter Suppression through Air Strakes.

By providing a minimum gap we can suppress flutter because the cushion pressure is kept low and the negative stiffness effect is less as shown by Equation (9) (or (19)). One of the ways of providing a minimum gap was employed successfully by Forzono (8). Another way may be to use a "corrugated trunk" as shown in Figure 38. In this case the strips are molded in the trunk in such a way that there are no sharp discontinuities. A third way is shown in Figure 39. In this configuration a plate-like structure is incorporated at the trunk bottom with holes in both vertical and horizontal directions. The vertical holes serve the function of the trunk orifices in providing air lubrication at the trunk bottom, whereas the horizontal holes provide vents for the cushion air.

78
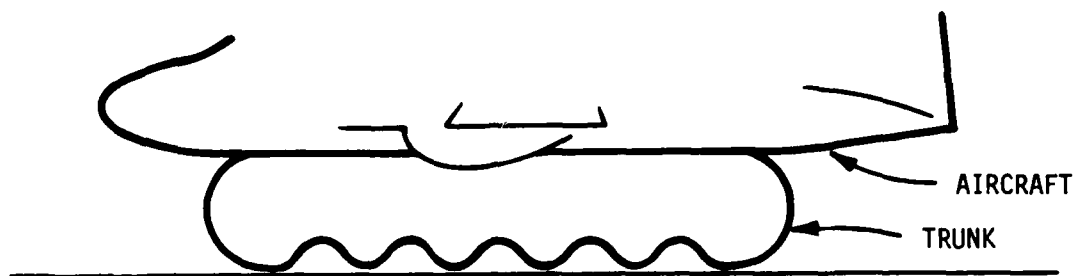
- SIMILAR TO FORZONO'S IDEA

- CORRUGATIONS CAST IN THE TRUNK TO PREVENT
  PEELING OFF

- THE DRAG MAY INCREASE SIGNIFICANTLY

Figure 38. Flutter Suppression through Corrugated Trunk.

One final way to modify the flow is to design ACLS so that the negative stiffness is much lower than the positive stiffness at operating condition. This way, by changing the operating condition, the flutter is suppressed.

All but two of these generic options are simulated using the computer program developed as part of the project (1). The only options not simulated are those of employing the circular trunk and the hybrid trunks because the computer program does not have provision for including hoop tension or the characteristics of a skirt.
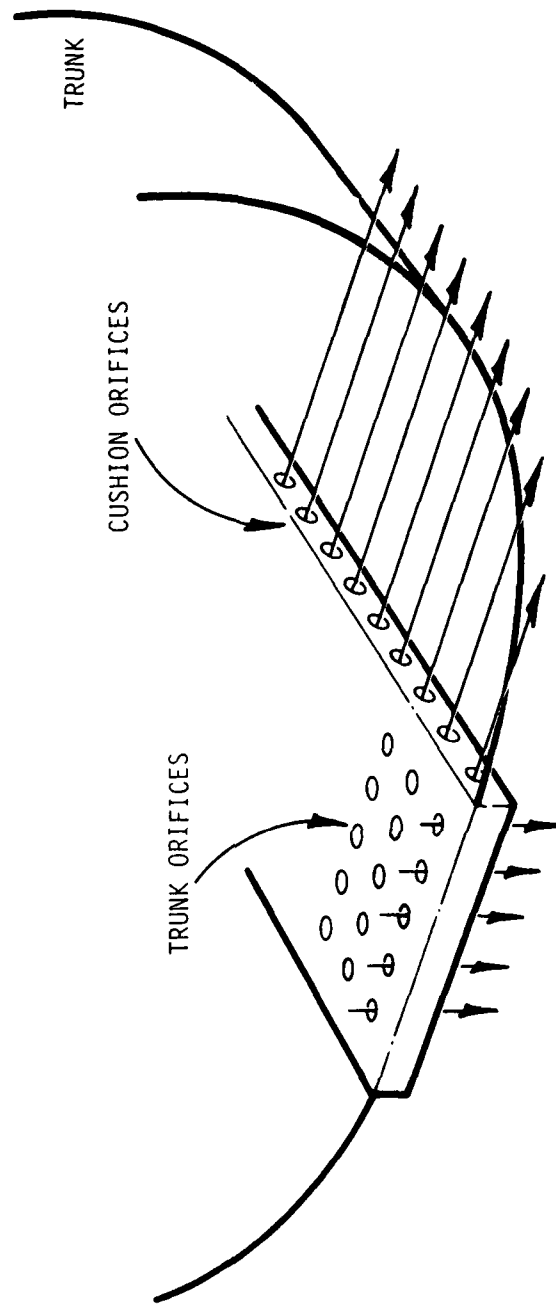
Figure 39. A Cross Tube Layer at the Trunk Bottom to Suppress Flutter.

TRUNK

CUSHION ORIFICES

TRUNK ORIFICES

5.2 Simulation of Trunk Flutter Solution Options

Many of the solution options suggested in the above subsection
can be simulated with minor modifications to the flutter model.
These solutions have been evaluated in the following pages. Two
options that cannot be simulated without major modification are:

    a.   Increasing hoop tension

    b.   Incorporating hybrid trunk.

5.2.1 Increasing Stiffness at Bottom

Both the tuned damper and the internal spring can be rep-
resented by a spring attached to a node on the trunk bottom.
Figure 40 shows one such spring for which the simulation was run.
Because of a horizontal component in the spring stiffness, it
represents the internal spring and not the tuned damper.

The trunk motion resulting from use of such a constraint
with the initial conditions identical to those for Case 2 in the
previous section is shown in Figure 41. As can be seen, the
spring has reduced the trunk flutter. However, as shown in the
continuation of the figure, the trunk node-12 exhibits a 10 Hz,
0.3 in. peak-to-peak motion which dies in a couple of cycles.

5.2.2 Increasing Flexural Stiffness

Increasing the flexural stiffness did not show much improve-
ment in the flutter characteristics. As shown in Figures 42 and
43 the flutter characteristics are not changed much when k_ℓ is
increased to 0.396 lb-ft^2/rad (k_ℓ is assumed to be zero for the
XC-8A trunk) and the flutter becomes more violent when it is
increased to 1.0 lb-ft^2/rad. This may be due to modifications
in the flow due to this trunk modification suggestion; namely,
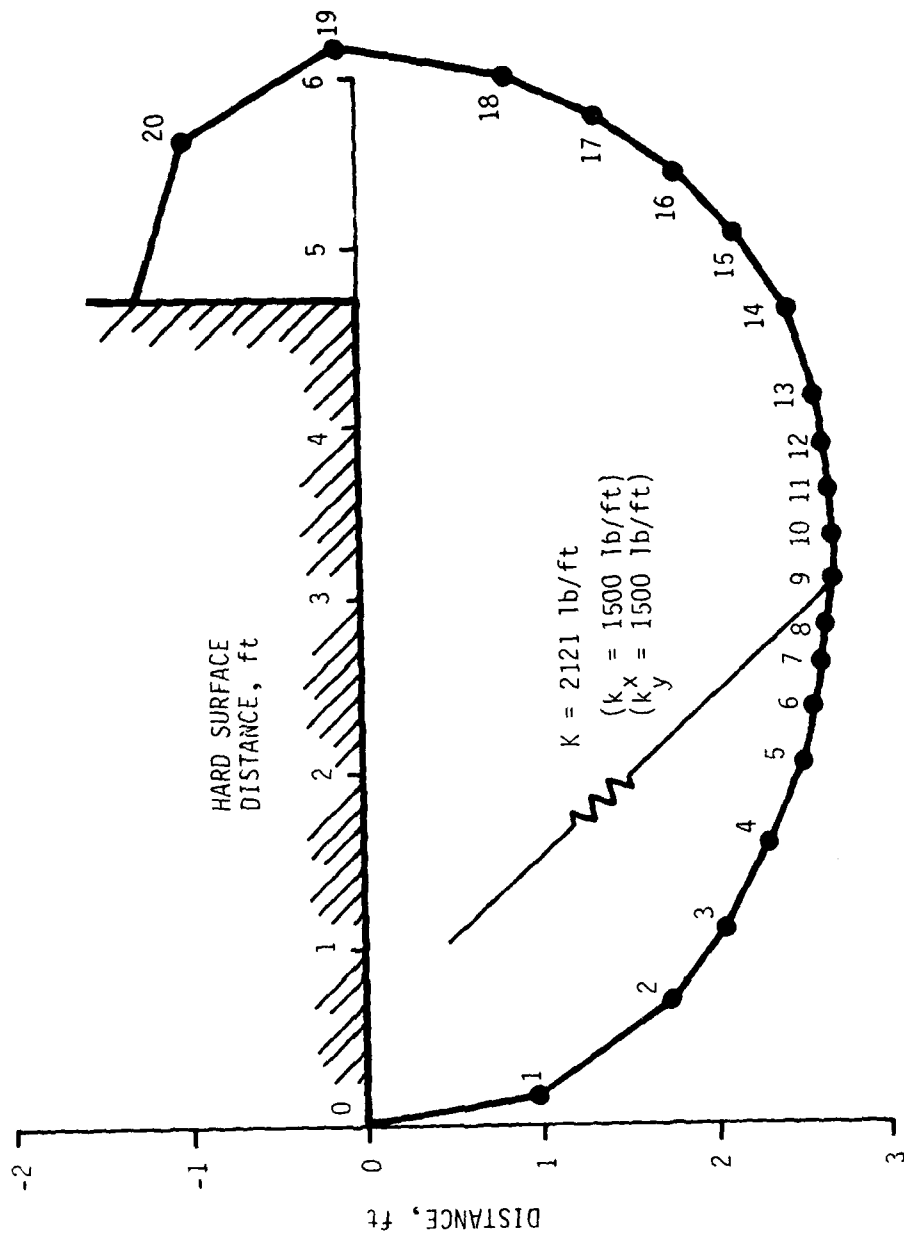the cushion air is even less easily vented out due to the increased

Figure 40. Location of Nodes and the Spring for the External Spring Case.

AD-A079 008   FOSTER-MILLER ASSOCIATES INC WALTHAM MASS   F/G 1/3
                ANALYSIS OF TRUNK FLUTTER IN AN AIR CUSHION LANDING SYSTEM.(U)
                AUG 79   A B BOGHANI, R B FISH   F33615-78-C-3412
UNCLASSIFIED   WP-7819   AFFDL-TR-79-3102   NL
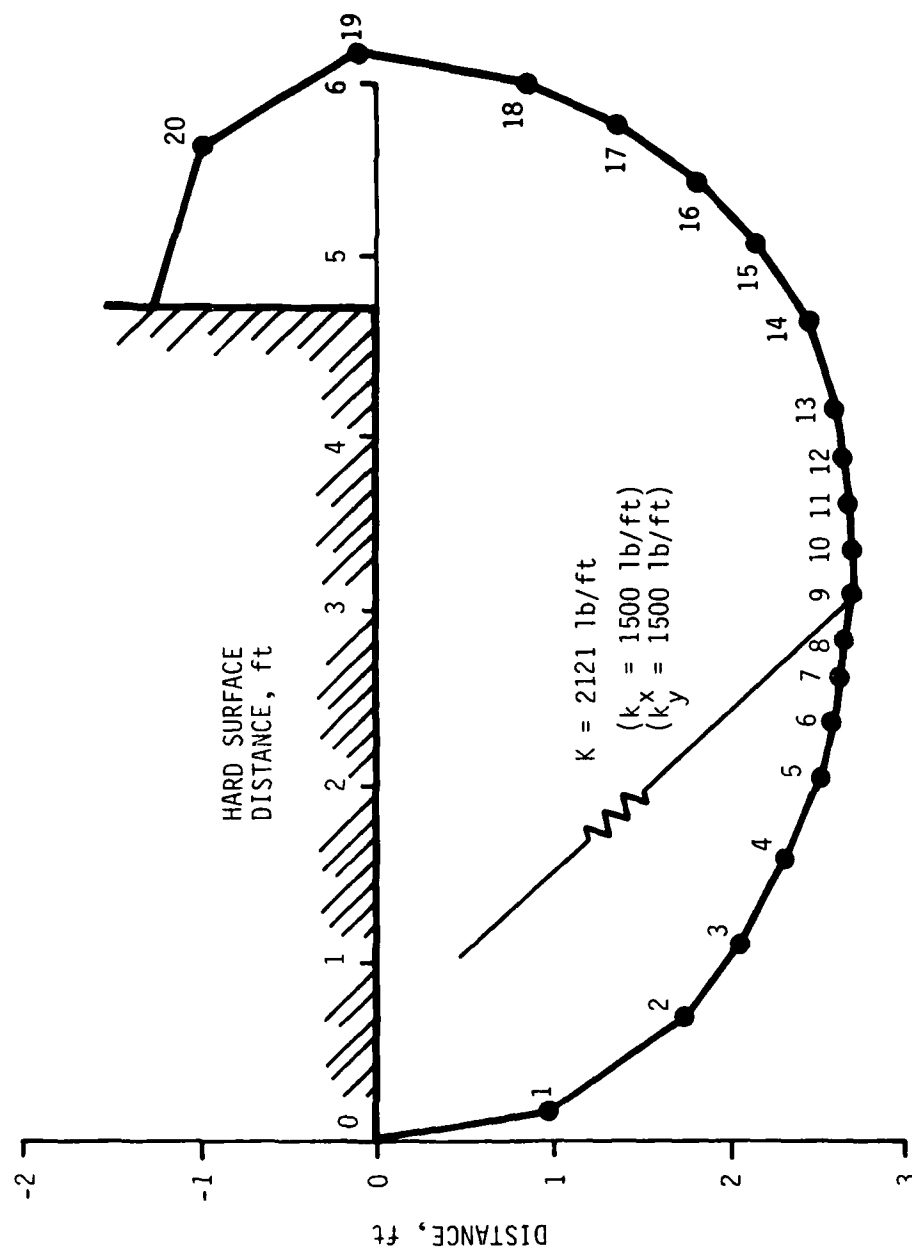
END
DATE
FILMED
2 80
DTIC

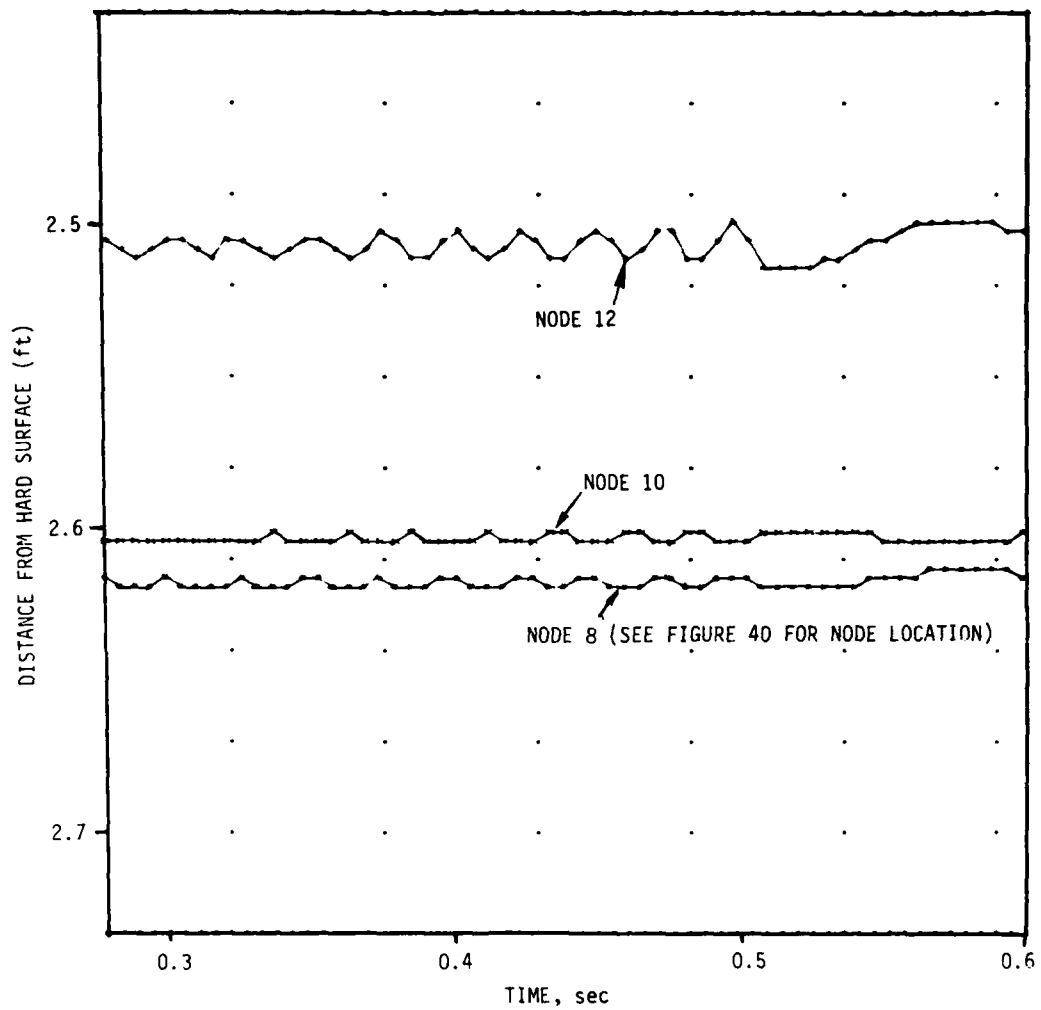Figure 40. Location of Nodes and the Spring for the External Spring Case.

82

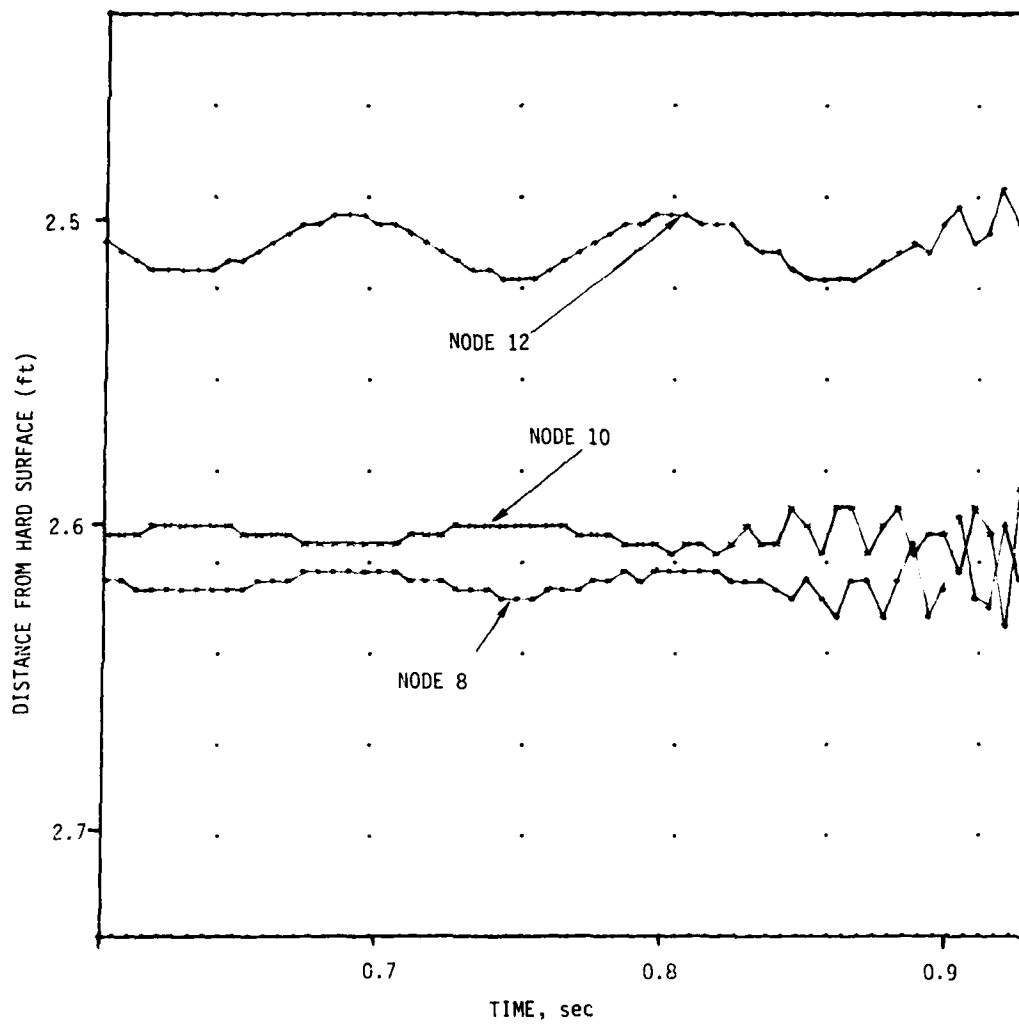Figure 41. Suppression of Flutter Due to External Spring Shown in Figure 40.

Figure 41. Suppression of Flutter Due to External Spring Shown in Figure 40 (Continued).
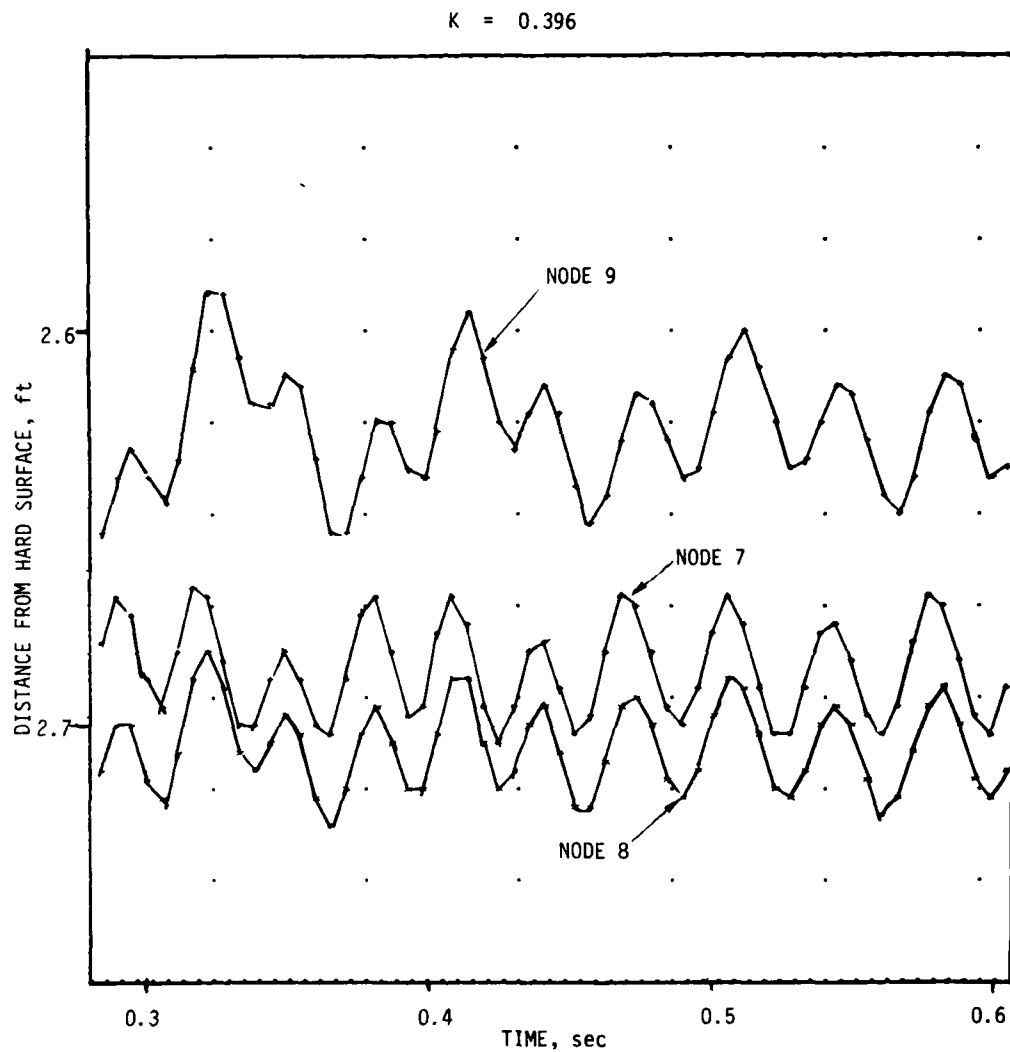
84

Figure 42.   Flutter Characteristics Due to Increase in Flexural
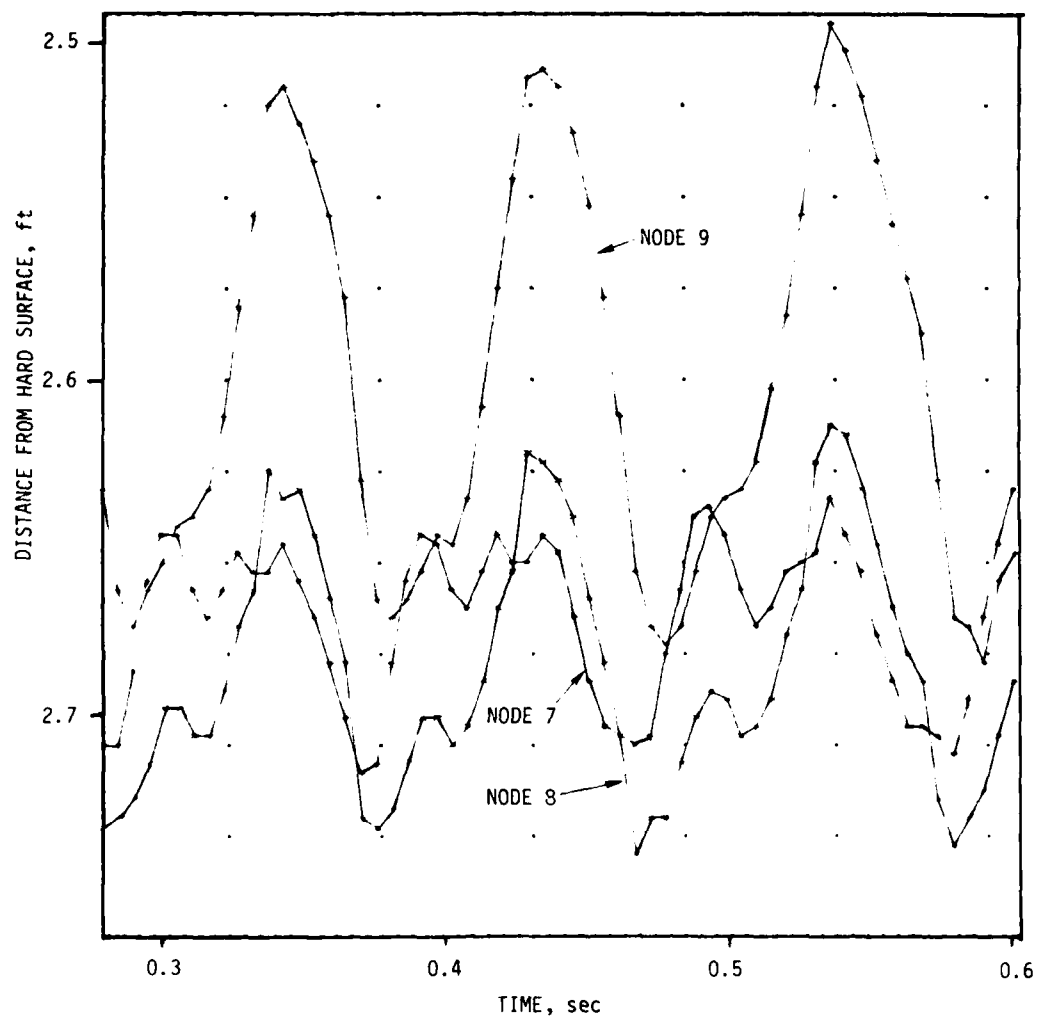Stiffness for k_ℓ = 0.396 lb-ft^2/rad.

85

Figure 43.   Flutter Characteristics Due to Increase in Flexural Stiffness to $k_\ell = 1.0$ lb-ft^2/rad.

86

resistance by the trunk. In addition, since increasing the flexural stiffness also increases weight of the trunk and makes it more difficult to retract, this option is not recommended.

5.2.3 Lowering the Separation Point

The separation point can be lowered either through a strake or through an "air strake" as discussed earlier. If the separation point is lowered and fixed to node 9 of the trunk, the flutter exhibited in Case 2 is suppressed as shown in Figure 44.

5.2.4 Providing a Minimum Gap

If the trunk is modified so that there is a minimum gap under the trunk to vent out the cushion air, flutter can be suppressed. This is demonstrated in Figures 26, 27 and 28 which shows absence of any node motion if the trunk bottom (on the trunk sides) is kept at least 0.1 ft off the ground.

5.2.5 Changing Operating Condition

This simple solution to the flutter problem can normally be implemented only during the design phases. If the ACLS parameters are adjusted so that the negative stiffness due to the flow does not exceed the positive stiffness due to the trunk tension, flutter may not be initiated. This is demonstrated by Figure 45 which shows absence of flutter in XC-8A if the hard surface clearance is increased to 2.9 ft accompanied by a drop in the cushion pressure to 90 psfg.
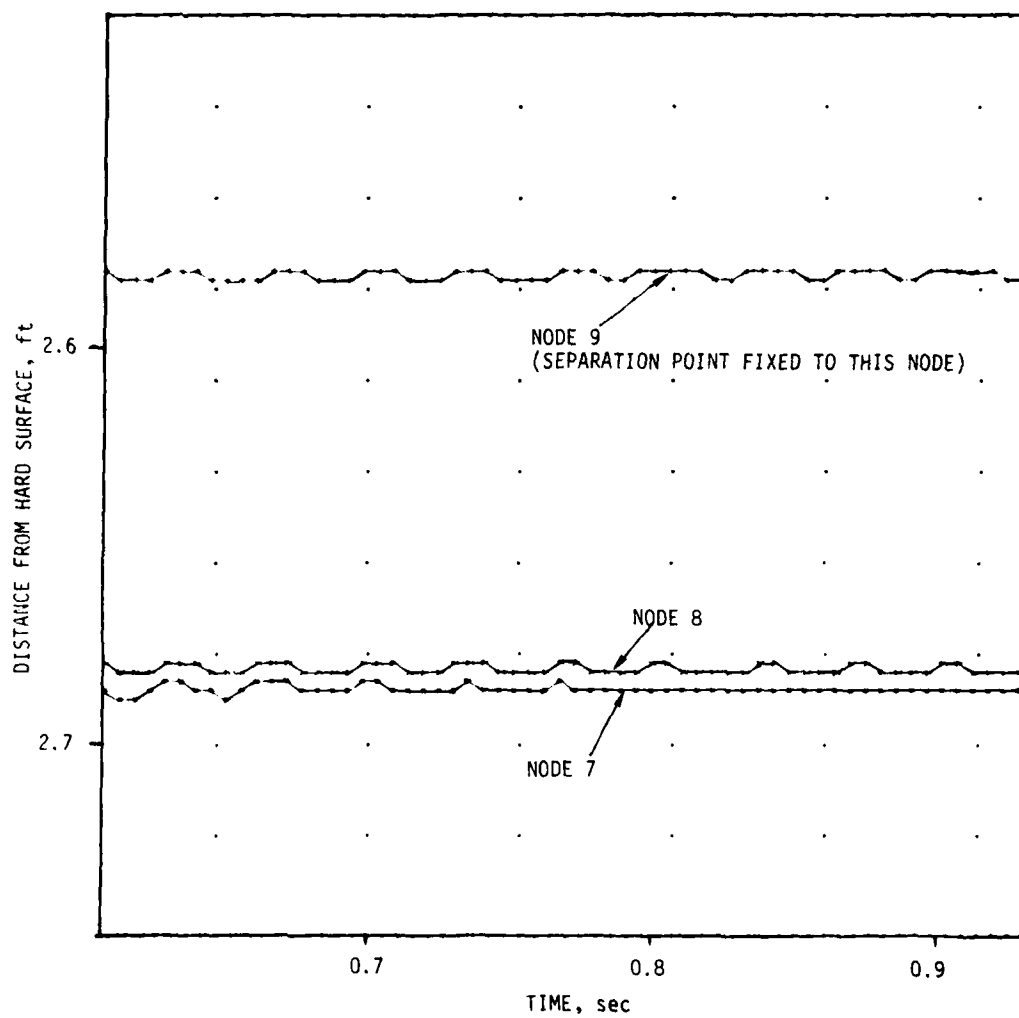
Figure 44. Suppression of Flutter Due to Lowering
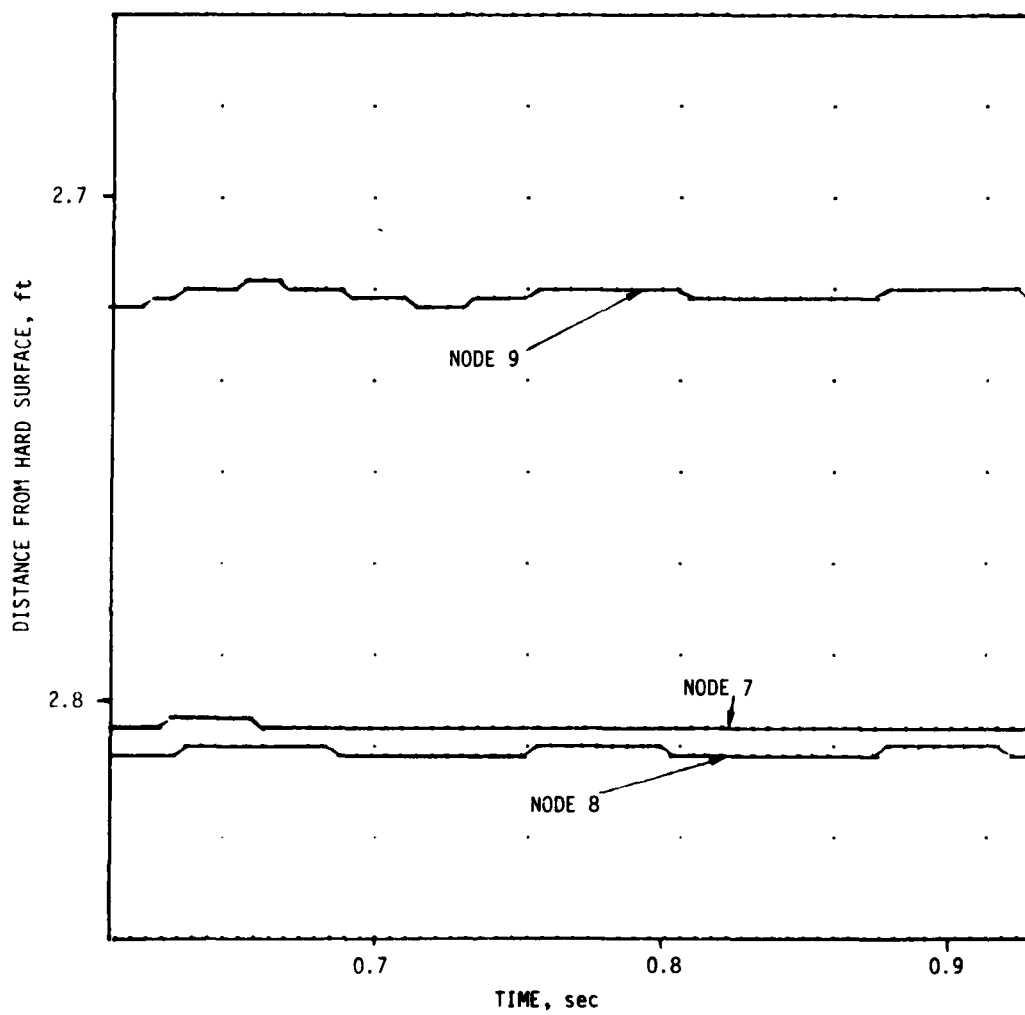Separation Point to Node 9.

88

Figure 45.   Flutter Suppression Due to Changes in the
             Operating Condition.

6. CONCLUSIONS AND RECOMMENDATIONS

The work performed under this contract has shown that the trunk flutter in ACLS is caused by a negative stiffness effect of flow under the trunk. This negative stiffness, if larger than the positive stiffness due to trunk tension, will initiate flutter. Comparing the results obtained using a computer program developed based on this model with the results from an XC-8A test verifies this explanation of flutter and demonstrates the effectiveness of the model in predicting flutter.

Based on this mechanism of flutter, several ways of eliminating it have been proposed. These various flutter suppressing concepts can be classified into two generic categories:

    a.   Modifying trunk

    b.   Modifying flow.

Initial simulations using the computer program have demonstrated the flutter reducing ability of the following three concepts within the above two categories.

    a.   Lowering separation point

    b.   Providing a minimum gap

    c.   Changing operating condition.

Two other options simulated have not proven to be very promising.

    a.   Increasing stiffness at bottom

    b.   Increasing flexural stiffness.

Although this work represents a strong initial effort, several tasks need to be performed in order to solve the flutter problem, for example:

a. Additional tests are needed to determine the location of the separation point during flutter. An improved separation point model will increase the accuracy of the computer program.

b. Further experimental investigations are needed to study the suggested flutter solutions. In particular the "hybrid trunk" mentioned in Section 5 should be investigated because it provides a fundamental improvement in the ACLS design in which the role of the trunk as a containment wall is eliminated; a role which leads to a variety of problems such as trunk flutter and trunk wear.

REFERENCES

1.   Anon., "Trunk Flutter Analysis, Program User's Manual," Submitted by Foster-Miller Associates, Contract No. F33615-78-C-3412, WPAFB, 1979.

2.   Lamb, H., "Hydrodynamics," Dover Publications, NY, 1945.

3.   Milns, Peter and Lloyd Gardner, "A-4 Twin Pod Air Cushion Test Specimen," D180-15370-1, The Boeing Co., 1973.

4.   Vaughan, John C., etal, "Laboratory Tests of an Air Cushion Recovery System for the Jindink Aircraft," AFFDL-TR-74-64, April 1974.

5.   Mayer, A. H., "A Study of Operational Problems of the XC-8A Air Cushion Landing System," AFFDL, March 1975.

6.   Bass, R. L., and J. E. Johnson, "An Experimental Study of Skirt Flutter on Surface Effect Take-off Landing (SETOL) Craft," Prepared by SWRI, Contract N62269-73-C-0216, Naval Air Development Center, Warminster, PA, June 1973.

7.   Han, Lit S., "An Analysis of ACLS Trunk Flutter," Ohio State University Research Foundation, August 1976.

8.   Forzono, C. J., "An Experimental Investigation of Trunk Flutter of an Air Cushion Landing System," AFFDL-TR-75-107, M.S. Thesis, The Ohio State University, March 1975.

9.   Fowler, H. S., "A Method of Controlling Skirt-Buzz," National Research Council, Div. of Mechanical Engineering, Engine Laboratory, Report No. LTR-ENG-13, November 1971.

10. Earl, T. D., "Air Cushion Landing Gear Applications Study," NASA Contractor Report CR159002, NASA, Langley Research Center, April 1979.

11. Boghani, A. B. and R. B. Fish, "Air Cushion Landing System Program FMA-4, Static and Dynamic Simulation of Heave-Pitch-Roll Motion: Computer Program Manual," LAR-12303, COSMIC, University of Georgia, Athens, GA, 1978.

12. Thompson, Wm. C., Ashok B. Boghani and Trafford J. W. Leland, "Experimental and Analytical Dynamic Flow Characteristics of an Axial-Flow Fan from an Air Cushion Landing System Model," NASA TN D-8413, NASA, Washington D.C., July 1977.

13. Roark, Raymond J., and Warren C. Young, "Formulas for Stress and Strain," 5th Ed., McGraw-Hill Book Co., N.Y., 1975.

14. McLintock, F. A., and A. S. Argon, "Mechanical Behavior of Materials," Addison-Wesley, 1966.

APPENDIX A

PRELIMINARY SEPARATION POINT AND
PRESSURE PROFILE TESTS

The objectives of these tests were twofold:

- Obtain a rough estimate of where the separation point lies

- Verify the use of Bernoulli's equation in determining the pressure profile under the trunk.

In order to obtain the location of the separation point on the ACLS at FMA, tufts were attached under the trunk as shown in Figure A-1. As can be seen, the tufts give some indication
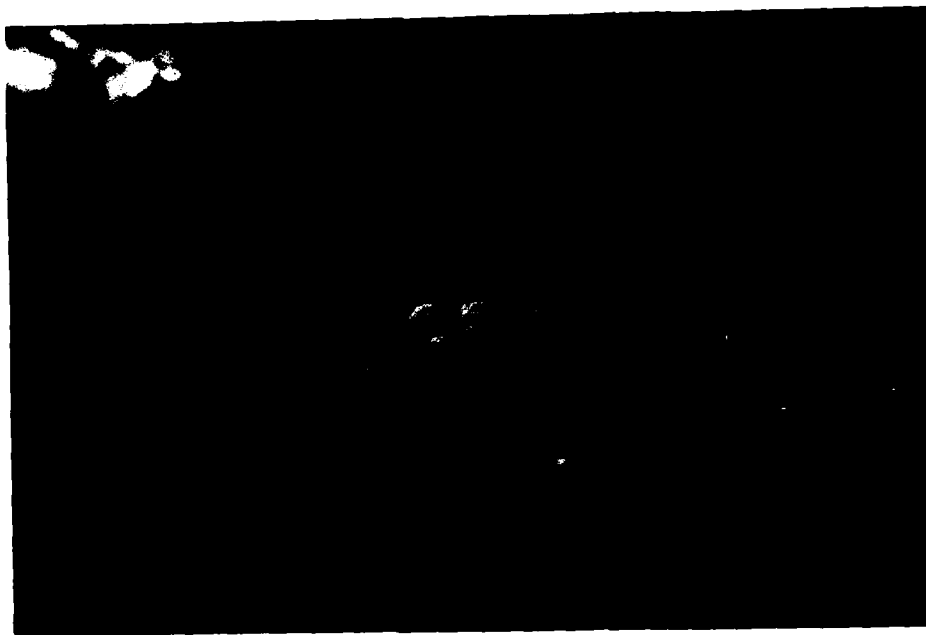

Figure A-1. Use of Tufts to Visualize Flow Field
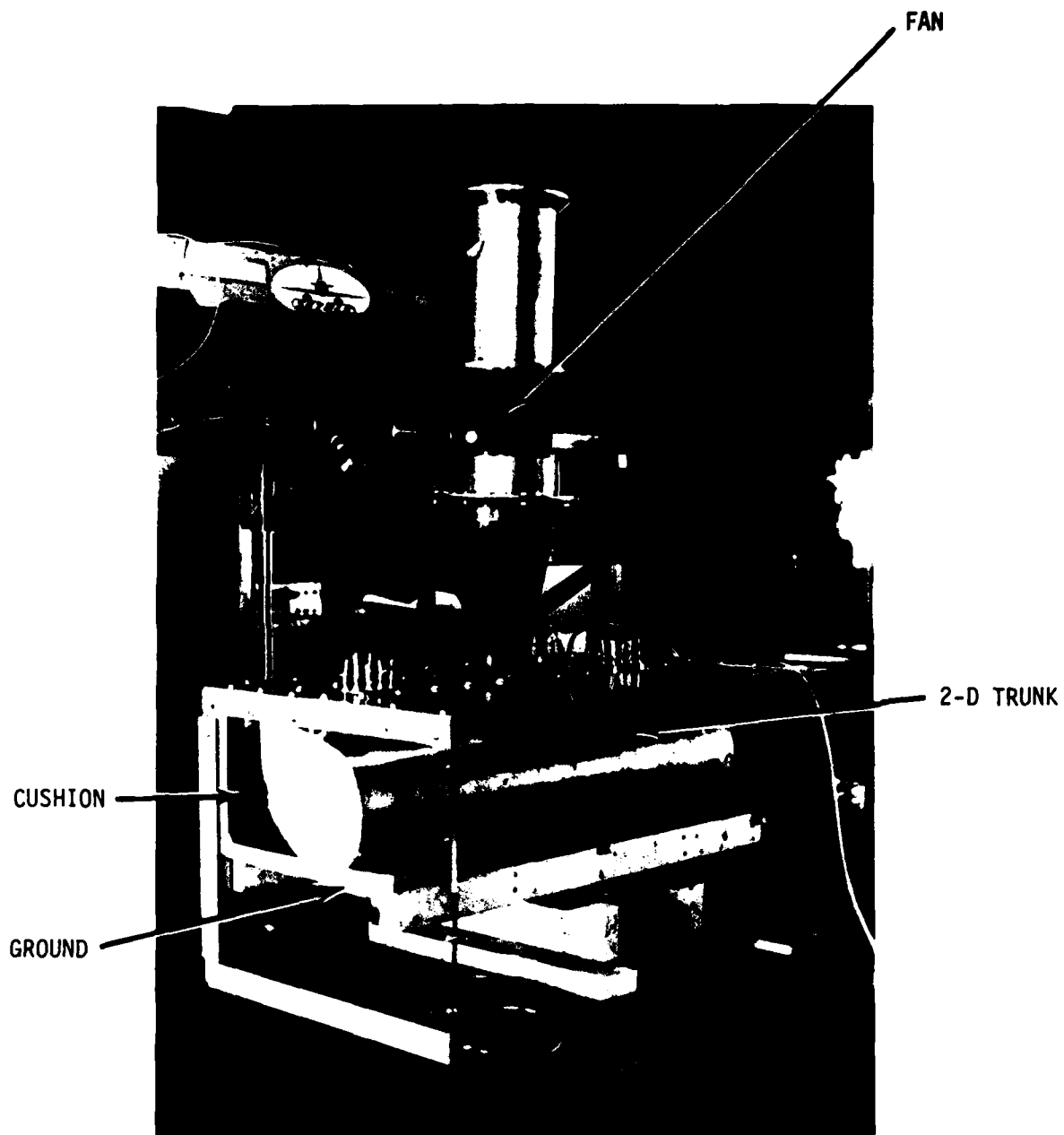on the Outer Side of the Trunk.

Figure A-2. The 2-D Rig used to obtain Separation Point and Pressure Profile.

of the flow pattern on the outside of the trunk. However, the difficulties in accurately identifying the separation point led to another test for determining its location.

In order to conduct the second test, the two-dimensional rig at FMA was modified to accommodate a trunk section made of thin steel plate with the same dimension as the sides of the prototype ACLS at FMA. As shown in Figure A-2 the sheet serves as an inflexible trunk which maintains a predetermined profile. A number of pressure taps were attached on the inside of the trunk in order to measure the pressure on the trunk surface, as shown in Figure A-3.

Powered by a Tech Development Tip Turbine fan, a trunk pressure of 45.7 psfg and cushion pressure of 20.8 psfg were achieved for the ground clearance of 5/32 in. The pressure profile obtained in this test is shown in Figure A-4. From the pressure profile the separation point was assumed to lie at tap No. 10 which is close to the 12 deg slope assumed in the simulation.

The pressure profile thus obtained was compared with that calculated applying Bernoulli's equation (that is, equation (6) in Section 3). As shown in Figure A-4 the measured pressure profile agreed very well with that predicted, thus proving the validity of the model.

If the gap is reduced, the pressure under the trunk reduces further as shown in Figure A-5. This reduction in pressure causes the negative stiffness effect which forms the basis of the trunk flutter model.
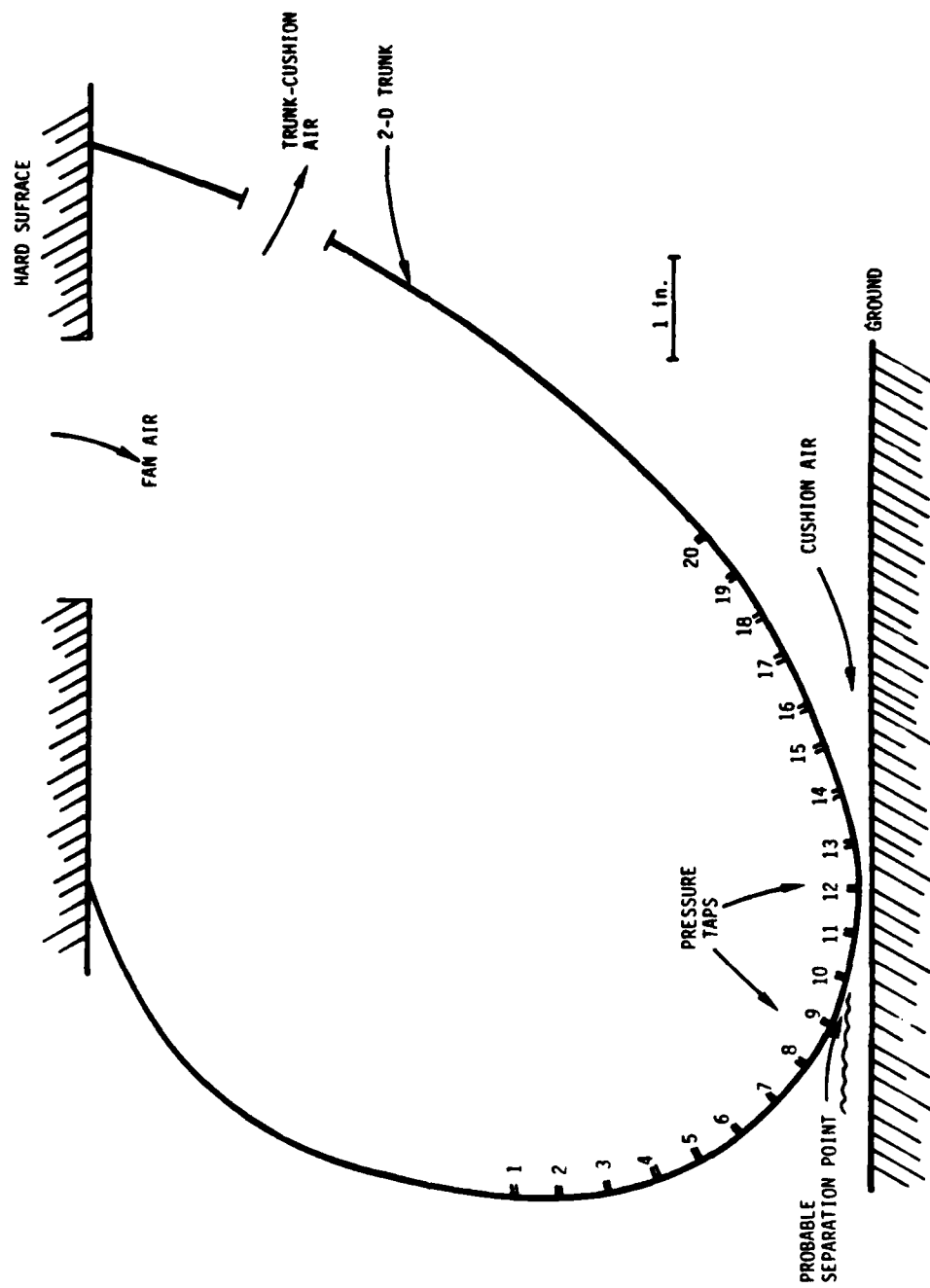
Figure A-3. Shape of the 2-D Trunk and Location of the Pressure Taps.
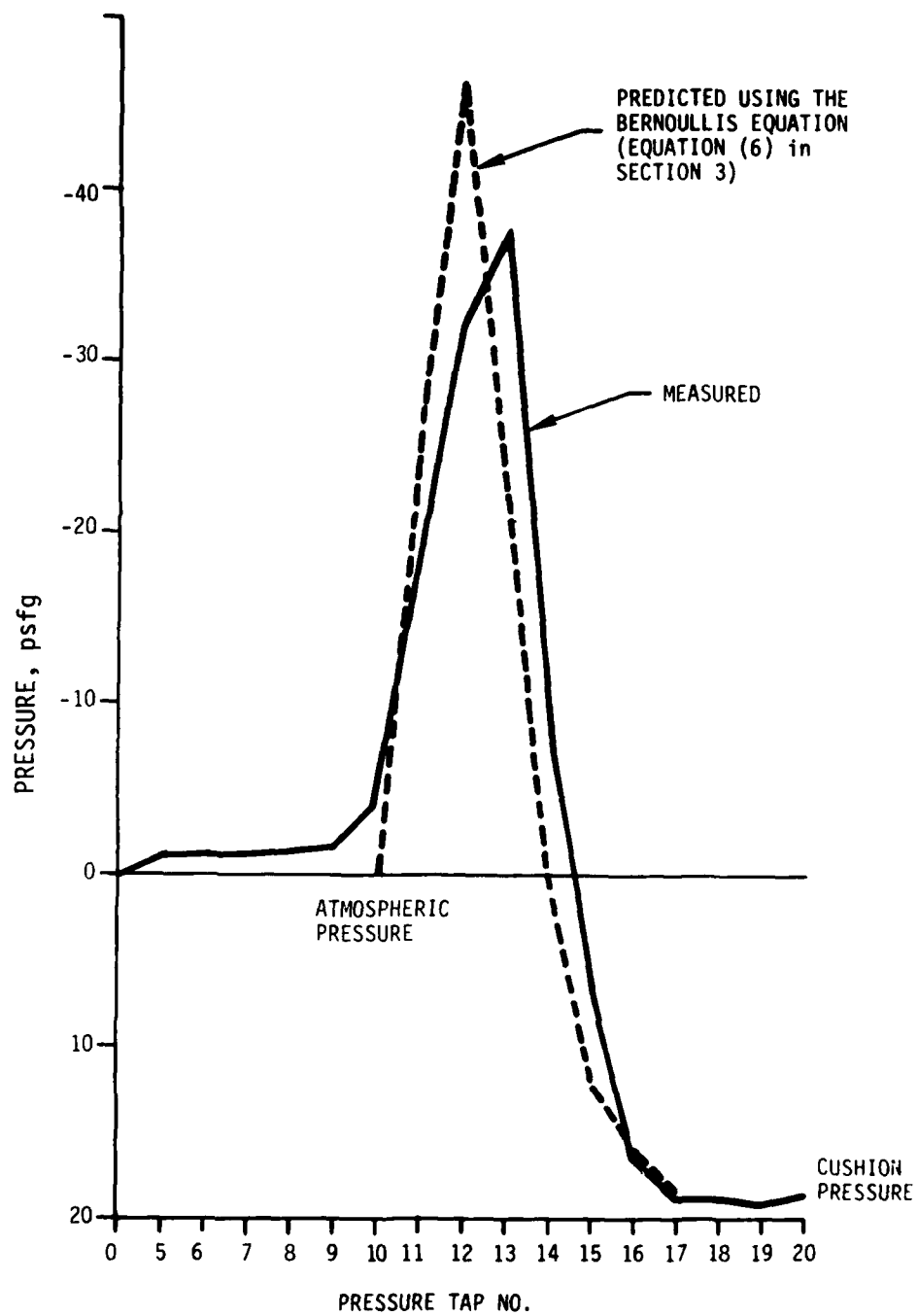
Figure A-4. Pressure Profile on the Experimental
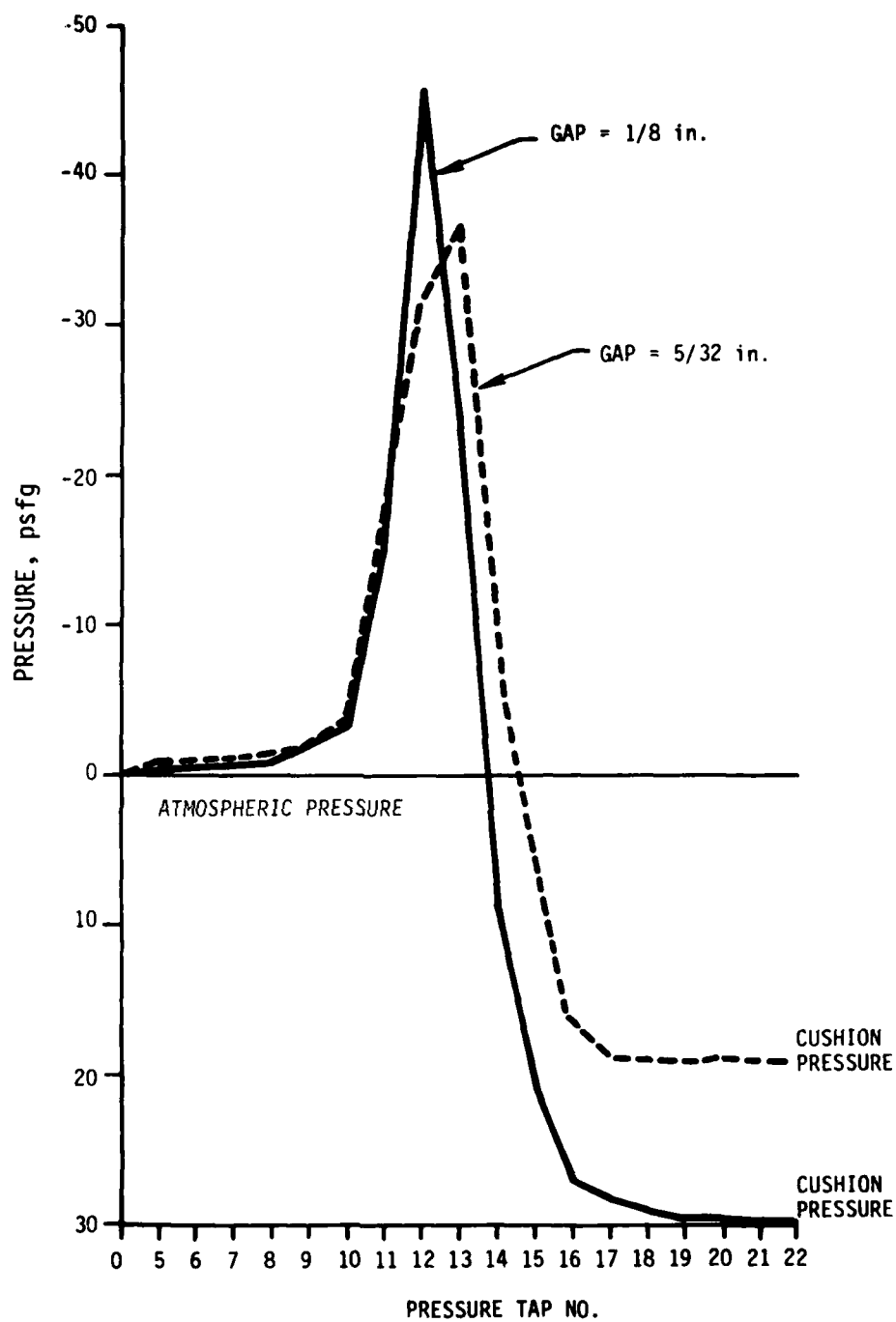Trunk Surface.

98

Figure A-5. Variations in the Measured Pressure Profiles
for Different Gap Heights.